JACS
JOURNAL OF THE AMERICAN CHEMICAL SOCIETY

Article

pubs.acs.org/JACS

# Mixed 14/16 Helices in the Gas Phase: Conformation-Specific Spectroscopy of Z-$(Gly)_n$, $n$ = 1, 3, 5

Jacob C. Dean, Evan G. Buchanan, and Timothy S. Zwier*

Department of Chemistry, Purdue University, West Lafayette, Indiana 47907-2084, United States

Supporting Information

**ABSTRACT:** Single-conformation ultraviolet and infrared spectroscopy has been carried out on the neutral peptide series, Z-$(Gly)_n$-OH, $n$ = 1,3,5 (ZGn) and Z-$(Gly)_5$-NHMe (ZG5-NHMe) in the isolated environment of a supersonic expansion. The N-terminal Z-cap (carboxybenzyl) provides an ultraviolet chromophore for resonant two-photon ionization (R2PI) spectroscopy. Conformation-specific infrared spectra were recorded in double resonance using resonant ion-dip infrared spectroscopy (RIDIRS). By comparing the experimental spectra with the predictions of DFT M05-2X/6-31+G(d) calculations, the structures could be characterized in terms of the sequence of intramolecular H-bonded rings of varying size. Despite the enhanced flexibility of the glycine residues, a total of only six conformers were observed among the four molecules. Two conformers for ZG1 were found with the major conformation taking on an extended, planar $\beta$-strand conformation. Two conformers were observed for ZG3, with the majority of the population in a C11/C7/C7/$\pi$($g-$) structure that forms a full loop of the glycine chain. Both ZG5 molecules had their population primarily in a single conformation, with structures characteristic of the first stages of a "mixed" $\beta$-helix. C14/C16 H-bonded rings in opposing directions (N → C and C → N) tie the helix together, with nearest-neighbor C7 rings turning the backbone so that it forms the helix. $\varphi/\psi$ angles alternate in sign along the backbone, as is characteristic of the mixed, C14/C16 $\beta$-helix. The calculated conformational energies of these structures are unusually stable relative to all others, with energies significantly lower than the PGI/PGII conformations characteristic of polyglycine structures in solution and in the crystalline form, where intermolecular H-bonds play a role.

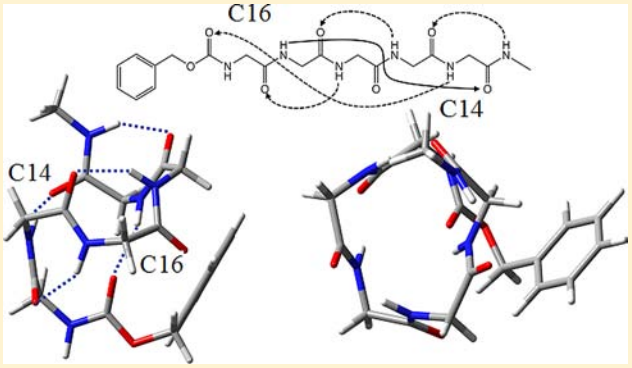


## 1. INTRODUCTION

The amino acids that make up proteins have distinct preferences for the secondary structures into which they fold in aqueous solution. For most amino acids, these preferences are influenced both by the intrinsic peptide backbone and the unique steric and structural constraints imposed by the side chain. If one is interested in the inherent preferences of the backbone itself, a natural place to start is with peptide sequences involving the simplest amino acid, glycine, which possesses no side chain, i.e. R = H, and consequently eliminates the $C_\alpha$ chiral center. Because of these properties, glycine residues are able to sample an unmatched range of Ramachandran angles,[1−3] allowing unusual structural flexibility.

One of the intriguing aspects of peptide secondary structural preferences is that these preferences are likely to be influenced significantly by different local environments, varying from the exposed polar solvent environment of aqueous solution to the nonpolar surroundings in cell membranes. The interactions that drive peptide conformations are remarkably different between the two, with peptide−water intermolecular interactions dominant in aqueous solution, but intrapeptide H-bonding dictating structural preferences in nonpolar environments such as membranes.

The conformations taken up by polyglycine in the condensed phase have been studied in some detail.[4−7] In its crystalline form two primary structures of polyglycine (PG) have been found: an extended $\beta$-sheet form known as PGI with Ramachandran angles (in degrees) nominally $\varphi$ = −150 and $\psi$ =+147, and a $3_1$-helix form known as PGII with approximately $\varphi$ = −77 and $\psi$ = +145.[4,5] In these forms of polyglycine, the unidirectional nature of the amide carbonyls increases the dipole moment of the polypeptide with increasing number of residues as the local amide dipoles add together. These structures are stabilized primarily by intermolecular H-bonds with neighboring polyglycine strands. In solution, the recent studies of Asher and co-workers have established that PGII structures dominate the solution-phase conformations, with slight variations about that central structure for larger oligoglycines.[5,6] Smaller glycine sequences ($n$ = 1−5) can adopt the PGI form, with some distribution between the two types.[5−7] Due to the limited solubility of the longer polyglycine chains, their aggregation behavior is also important. Recently, Lorusso et al. studied the assembly of polyglycine fibrils, with $\beta$-

**Received:** July 21, 2012
**Published:** October 5, 2012

   dx.doi.org/10.1021/ja306652c | J. Am. Chem. Soc. 2012, 134, 17186−17201

sheet conformations playing a dominant role.[8] These unbranched fibrils reflect amyloidogenic behavior with self-aggregation into unbranched amyloid-like fibrils.[8] Whether in solution, crystalline form, or as fibrils, the primary driving forces for polyglycine conformation are intermolecular H-bonds formed either with other polyglycine chains or with solvent.

Given the lack of steric constraints and large range of Ramachandran angles sampled by glycine residues, the effect of interactions with solvent may be particularly important for stabilizing secondary structure. It is therefore of interest to characterize in some detail the conformational preferences of homoglycine oligomers in the absence of solvent. Studying these molecules at low temperatures also enables the characterization of the energetically most-preferred conformers, which are low-lying minima on the potential energy surface. Such studies on homoglycines have focused on small peptides such as *N,N*-dimethylglycine neutral via microwave spectroscopy[9] and protonated diglycine, $(Gly)_2H^+$, via vibrational $H_2$/$D_2$ photofragment spectroscopy.[10,11] The mono- and dipeptides studied in these experiments are too short to observe the development of secondary structure, but they do show that nearest-neighbor preferences in the smallest glycine peptides are extended $\beta$-strand-like conformations characterized by C5 intramolecular interactions (five atoms in a H-bonded ring).

Several room temperature studies of protonated glycine oligomers have also been undertaken using mass spectrometric methods such as ion mobility[12] and infrared multiple-photon dissociation (IRMPD) spectroscopy.[13] However, the presence of the charge can perturb the structure significantly as nearby C=O groups bind to it. Furthermore, room temperature measurements necessarily sample a much broader distribution of conformations, each of which contributes to the infrared spectrum, complicating assignments.

There have been several computational investigations of polyglycines, with many studies comparing small oligomers in the extended $\beta$-strand conformation with common periodic secondary structures (repeating $\varphi/\psi$ angles) such as the $3_{10}$-helix,[14−16] $2_7$-ribbon (repeating C7 intramolecular H-bonded rings),[17] $\alpha$-helix,[18] and $\pi$-helix.[18] Full conformational analysis of the tripeptide Ac-$(Gly)_2$-NHMe predicted that C10 and C7 intramolecular H-bonded structures would be most stable.[19]

Among these studies, the work of Baldauf et al.[15,16] is notable in that it identified and characterized a nonstandard helix that could be formed by polyglycine chains, referred to as a "mixed" $H_{14/16}$ helix, composed of alternating C14 and C16 H-bonded rings with a helical pitch of about 4 residues per turn. As an illustration, Figure 1b shows a 14/16 mixed helix structure for Ac-$(Gly)_6$-NHMe using the Ramachandran angles from Baldauf et al.[15,16] The alternation of H-bonded ring types is a characteristic feature of mixed helices (and is responsible for their classification as 'mixed'). Furthermore, in the $H_{14/16}$ mixed helix, the direction of the H-bonds alternates, N → C terminal and C → N terminal. In this sense, it has the characteristics of a $\beta$-helix,[15,16] with H-bonds that point in opposite directions, leading to a small permanent dipole moment relative to their unidirectional counterparts (e.g., PGI, PGII, $\alpha$-helix or $3_{10}$ helix). In so doing, Ramachandran angles along the peptide backbone alternate in magnitude and sign, (+80°, −60°) and (−60°, +80°).

Mixed helices are common in $\beta$-, $\gamma$-, and mixed $\alpha/\beta$- and $\alpha/\gamma$-peptides[15,16,20−22] but are quite uncommon in $\alpha$-peptides, particularly in aqueous solution.[23] At the same time, the predictions of Baldauf[15,16] and later MD simulations on longer

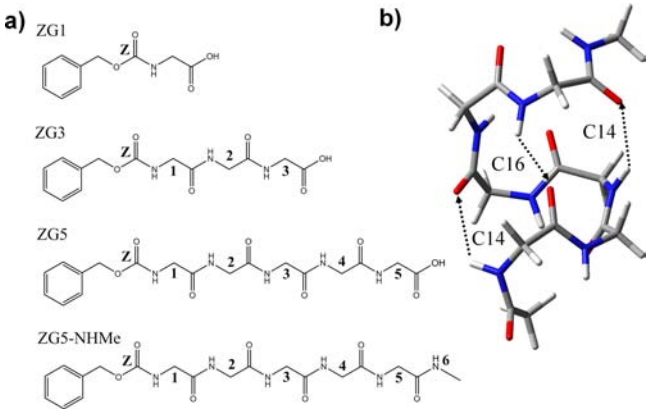


**Figure 1.** (a) Chemical structures of Z-$(Gly)_n$-OH, $n$ = 1, 3, 5 and Z-$(Gly)_5$-NHMe (top to bottom), where Z = benzylcarboxy cap and the numbers represent the residue number. (b) Ac-$(Gly)_6$-NHMe in the $H_{14/16}$ helix form using $\varphi/\psi$ angles calculated by Baldauf et al.[15] with C14 and C16 H-bonds shown as dotted lines.

polyglycine chains by Itoh et al.[24] predict that these mixed $H_{14/16}$ helices are significantly lower in energy than other model secondary structures in the gas phase or in low dielectric media. In fact free energy estimates predict that mixed helices should compete for population at room temperature in polyglycine chains with $n$ = 5−10 *in vacuo* or nonpolar solvents. However, these predictions have lacked direct experimental verification.

Gas-phase spectroscopic studies on small peptides have yielded valuable insight into local conformational preferences and the interactions that govern conformational stability within larger proteins. Supersonic expansion cooling coupled with IR/UV double resonance methods allows for intrinsic conformational preferences to be investigated in the absence of solvent thereby yielding information on the primary intramolecular forces leading the development of secondary structure. Several studies have probed the IR and UV spectroscopy of prototypical secondary structures in neutral $\alpha$-peptides, including $\beta$-turns,[25,26] $\gamma$-turns,[26−28] $\beta$-strands,[29] and the early stages of $3_{10}$-helix,[30,31] $\beta$-sheet,[29,32,33] and $\beta$-hairpin[34] formation. In our group, the inherent conformational preferences of a series of prototypical synthetic foldamers with extended carbon backbones have been explored, including $\beta$-peptides,[35,36] $\alpha/\beta$-peptides,[37,38] and $\gamma$-peptides.[39−41] At the same time, there are comparatively few conformation-specific studies[34,42,43] of neutral peptides with more than four residues due to the challenges they present to efficient laser desorption and cooling as the size of the molecule increases.

In this work, the neutral series Z-$(Gly)_n$-OH, $n$ = 1,3,5 (ZGn) and Z-$(Gly)_5$-NHMe (ZG5-NHMe) has been studied using IR−UV double resonance methods in a supersonic expansion. These structures are shown in Figure 1a. The Z (carboxybenzyl) cap on the N-terminus was chosen as a way to incorporate the near-UV chromophore required for IR/UV spectroscopy with minimal perturbation to the glycine peptide structure.[26,44] Using resonant two-photon ionization (R2PI) and IR−UV double resonance methods, we report conformation-specific IR and UV spectra for this series, shedding light on the developing intramolecular H-bonded network being formed. The broad coverage in the infrared, including both hydride stretch and amide I/II regions, provide complementary insights to the structures formed. As we shall see, all members of this series funnel their population into one or at most two conformations, suggesting an unusual stability for the


dx.doi.org/10.1021/ja306652c | J. Am. Chem. Soc. 2012, 134, 17186−17201

developing secondary structure. By comparing our results with the predictions of calculations, firm conformational assignments for these conformers are obtained. As we shall see, the pentaglycines show clear evidence for formation of the first stages of a mixed $H_{14/16}$ helix, providing an experimental foundation for the computational predictions of Baldauf and co-workers.[15,16]

## 2. EXPERIMENTAL SECTION

**2.1. Experimental Methods.** All of the Z-$(Gly)_n$-OH samples were purchased from Bachem, and Z-$(Gly)_5$-NHMe was synthesized from Z-$(Gly)_5$-OH using a common -NHMe capping procedure.[40] The samples were each brought into the gas phase by laser desorption from a graphite rod.[45] The desorbed molecules were entrained in a supersonic jet expansion of argon gas (5−6 bar backing pressure), pulsed at 20 Hz out of a series 9 General Valve nozzle with a 500−800 $\mu$m diameter orifice. The fundamental of a Nd:YAG laser (Continuum Minilite II) operating at 20 Hz was used for desorption at a pulse energy of 3−5 mJ/pulse with a 2 mm beam diameter. The sample was rubbed into the surface of a graphite block, and positioned underneath the nozzle orifice via a load-lock assembly. A linear motion actuator translated the graphite block to ensure exposure of new sample to the desorption laser. A more detailed explanation of the laser desorption source is given in the Supporting Information. The expansion was skimmed downstream, forming a molecular beam prior to entering the ionization region of a time-of-flight mass spectrometer.

Resonant two-photon ionization (R2PI) was used to attain mass-selected UV excitation spectra in the $S_0-S_1$ region. The UV photons used for one-color R2PI were generated by the frequency doubled output of a Nd:YAG (355 nm) pumped dye laser scanning from 265 to 268 nm at pulse energies of 0.1−0.3 mJ/pulse at a 20 Hz repetition rate. Conformation-specific IR spectra were obtained using resonant ion-dip infrared spectroscopy (RIDIRS)[46,47] in the NH/OH stretching region (3200−3650 $cm^{-1}$) and amide I/II (1450−1850 $cm^{-1}$) regions. These spectra were recorded by monitoring the ion signal of a unique vibronic transition in the UV, while scanning a Nd:YAG pumped parametric converter (LaserVision) operating at 10 Hz (idler energies ~15 mJ/pulse). The IR beam was spatially overlapped with the UV laser, but arrived 200 ns earlier. When resonant with an IR transition of the conformer of interest, the ground-state population of those molecules was depleted, appearing as a loss in the ion signal from the monitored vibronic transition. Given that the IR laser is operated at half of the repetition rate of the UV laser, the difference between IR "on" and IR "off" in the total ion signal was monitored directly using the active baseline subtraction mode of a gated integrator (Stanford Research). For generation of IR light in the amide I/II regions, a $AgGaSe_2$ crystal was fixed downfield of the OPO output, and pulse energies of 0.7−1.0 mJ/pulse were attained. All RIDIR spectra were obtained by monitoring the origin transition of each conformer in their respective UV spectra.

Conformation-specific UV spectra were recorded using IR−UV holeburning spectroscopy.[47] In this case, a unique infrared band observed in the RIDIR spectrum of a particular conformer was used to burn a hole in the UV-interrogated population. A configuration identical to RIDIRS was used, except that the UV laser was scanned while the IR laser was fixed. UV transitions of the conformer sharing the same ground-state level as the IR excited population appear in the spectrum. For all IR−UV HB spectra, multiple infrared transitions in the individual RIDIR spectra were checked to ensure that the IR band chosen for the holeburn transition was unique to a particular conformer of interest.

**2.2. Computational Methods.** To identify the possible conformational minima associated with each molecule studied, a conformational search was carried out for each molecule using the Amber* force field[48] in the MACROMODEL suite of programs.[49] Minima within a 50 kJ/mol energy window were recovered, and the lowest 60−100 unique structures within those results were selected for further optimization using density functional theory (DFT). DFT calculations were performed using the *Gaussian 09* suite of programs.[50] These calculations involved tight geometry optimizations followed by harmonic vibrational frequency calculations using the hybrid functional M05-2X[51] with the 6-31+G(d) basis set. M05-2X handles short-range dispersion effects that are not accounted for in common functionals such as B3LYP.[51] The harmonic frequency calculations aided in the assignment of conformational isomers observed in the experiment. These frequencies were scaled by 0.952 for OH stretch, 0.943 for NH stretch, and 0.960 for amide I/II frequencies to account for the expected differences in anharmonicity associated with each type of oscillator. These scale factors were chosen by scaling the calculated IR frequencies of the assigned structure of ZG1(A) to the experimental frequencies. This assignment was made confidently, and served as the basis for scaling the calculated frequencies for the other members of the ZGn series, as has been done in previous studies.[30,38,40,41,43,52,53] In the conformational assignment process, the vibrational frequencies for all optimized structures within 25 kJ/mol of the global minimum were checked against the experimental IR spectra to ensure valid assignments.

**2.3. Structural Considerations.** In analyzing the ZGn structures, a common nomenclature was used in referencing structural aspects of different conformations. First, as shown in Figure 1a, the numbering of specific NH and C═O groups is by glycine residue, proceeding from the N- to the C-terminus. For instance, in the ZG3 structure shown in Figure 1, the NH and CO groups with the label "2" on the $CH_2$ between them are labeled NH[2] and CO[2] in the text. Similarly the Ramachandran $\varphi/\psi$ angles about the NH[2]−$CH_2$[2] and $CH_2$[2]−CO[2] bonds are labeled $\varphi_2$ and $\psi_2$. The C═O on the Z-cap is simply denoted as "CO[Z]." The orientation of the phenyl ring with respect to the glycine chain was designated by the $C_{phe}C_{\alpha}OC(O)$ dihedral angle, with *gauche*+ (g+) referring to dihedrals $0 \leq \chi \leq +120°$, *gauche*− (g−) for $-120° \leq \chi \leq 0°$ and anti (a) for $120° \leq \chi \leq 240°$. Hydrogen-bonding patterns are described in terms of the specific H-bond type, and are labeled by the respective NH/OH groups going sequentially from the N → C terminus (NH[1]/NH[2]/NH[3]/OH for ZG3). Most H-bonds observed were H-bonded rings, and are characterized by the total number of atoms, *n*, within the ring that tie together the N−H···O═C groups. These are labeled as "C*n*." $\pi$ H-bonds are simply labeled "$\pi$," and groups not H-bonding are labeled "f" for free. It should also be noted that since no chiral centers exist in glycine, individual structures have an equivalent with all $\varphi/\psi$ angles with opposite sign.

## 3. RESULTS

**3.1. Z-Gly-OH (ZG1).** *3.1.1. R2PI and IR−UV HB Spectroscopy.* The R2PI spectrum and IR−UV HB spectra for ZG1 are shown in Figure 2. The R2PI spectrum shows one dominant transition at 37601 $cm^{-1}$ with a smaller shoulder approximately 3 $cm^{-1}$ to the red. As displayed in the IR−UV HB spectra, these two transitions are due to $S_0-S_1$ origin transitions for two conformers, labeled A and B respectively. Each conformer has a small vibronic band 17 $cm^{-1}$ from their origin, tentatively assigned to a butterfly motion between the phenyl ring and glycine chain based on vibrational frequency calculations of the assigned conformers (section 3.1.2). The small bands labeled with asterisks in the R2PI spectrum are hot bands.

*3.1.2. RIDIR Spectroscopy.* Figure 3 presents the RIDIR spectra for conformers A and B in the NH/OH stretch region (a and b) as well as the amide I/II region (c and d). Conformer A has hydride stretch bands at 3472 $cm^{-1}$ and 3585 $cm^{-1}$ respectively, which fall in the spectral ranges for a nearly free amide NH and free carboxylic acid OH. The amide NH frequency is slightly blue-shifted from a typical C5 amide NH stretch (~3450 $cm^{-1}$), due to the unique OC(═O)NH environment of the Z-cap. A summary of the wavenumber positions (in $cm^{-1}$) of the experimental transitions in the NH/

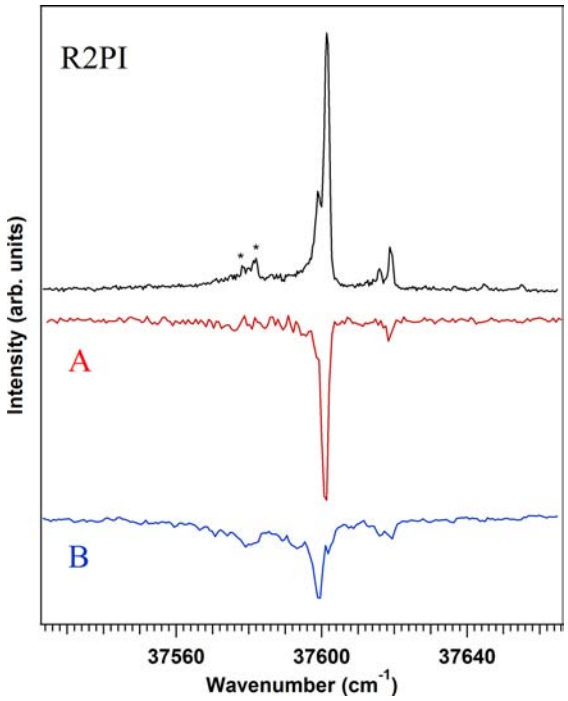


**Figure 2.** R2PI spectrum of Z-Gly-OH (top trace) and IR–UV HB spectra of the observed conformers (A and B). Asterisks in the R2PI spectrum indicate hot bands. The IR transitions used for the holeburn spectra were those at 3472 and 3466 $cm^{-1}$ respectively.

OH stretch, amide I and amide II regions is included in the Supporting Information (Table S1).

Since the $S_0$–$S_1$ origin transition of B appears as a shoulder on A and was used as the monitor transition (Figure 2), the RIDIR spectra of B contained a contribution due to A, which needed to be subtracted out to obtain the true spectrum of conformer B. The resulting spectrum due to conformer B is nearly identical to that of A, with small shifts to lower frequency in both the NH and OH stretch fundamentals (by −5 and −1 $cm^{-1}$, respectively). The calculated spectra (shown as sticks) replicate the experimental features, including the subtle frequency shifts between conformers and the intensity differences between bands. The structure corresponding to ZG1(A) is shown to the left in Figure 4a. The planar, extended

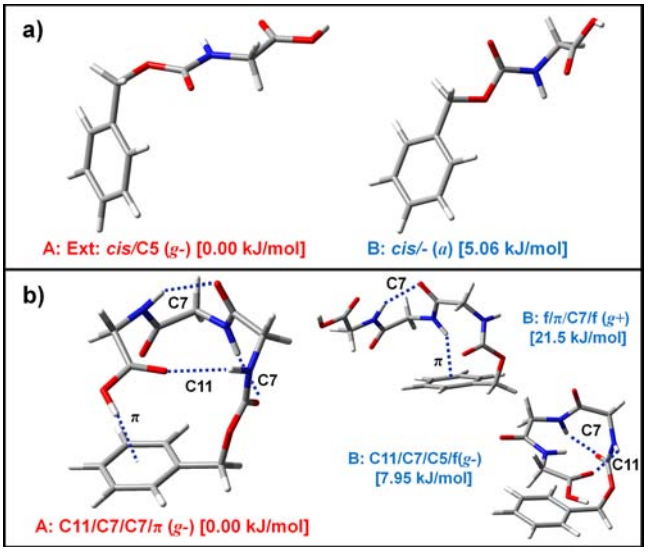


**Figure 4.** Assigned structures for observed conformers of (a) Z-Gly-OH and (b) Z-$(Gly)_3$-OH showing the H-bonding patterns with labels. Structures were calculated using DFT at the M05-2X/6-31G +(d) level of theory.

*β*-strand structure has a weak C5 interaction between the amide NH and carboxylic acid C═O (*cis*), with the phenyl ring in the g− position. The structure assigned to ZG1(B) has an anti Z-cap arrangement (Figure 4a) with the carboxylic acid bent out of the glycine plane. The *cis* arrangement of CO[1] and NH[1] is retained. The asterisks on the NH stretch bands in Figure

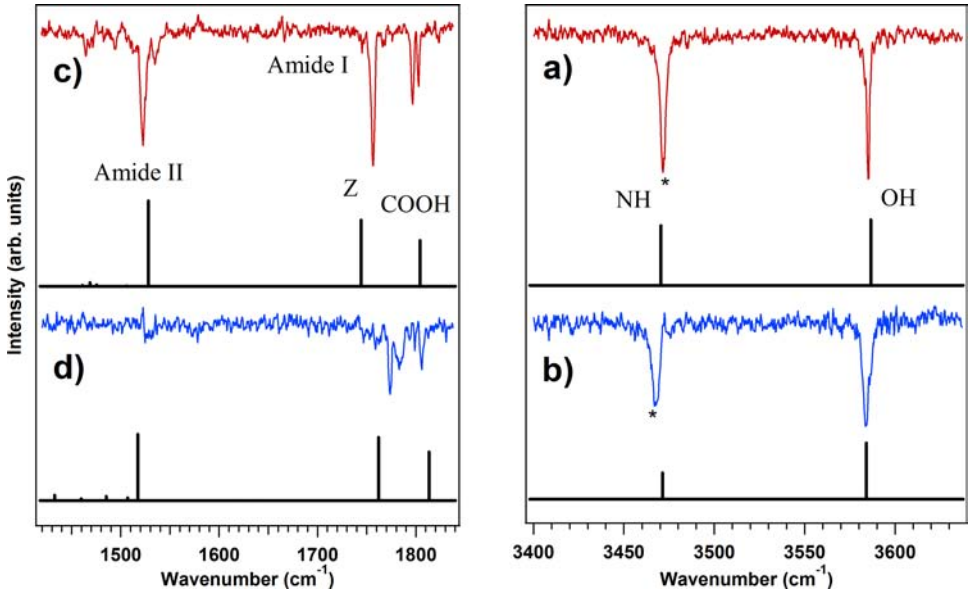


**Figure 3.** Z-Gly-OH amide I/II (left) and NH/OH stretch (right) RIDIR spectra for conformers A (upper) and B (lower) with calculated IR spectra calculated at the DFT//M05-2X/6-31+G(d) level of theory using scaling factors of: 0.96 (amide I/II), 0.943 (NH stretch), 0.952 (OH stretch). Asterisks indicate IR–UV holeburn transitions.


dx.doi.org/10.1021/ja306652c | J. Am. Chem. Soc. 2012, 134, 17186–17201

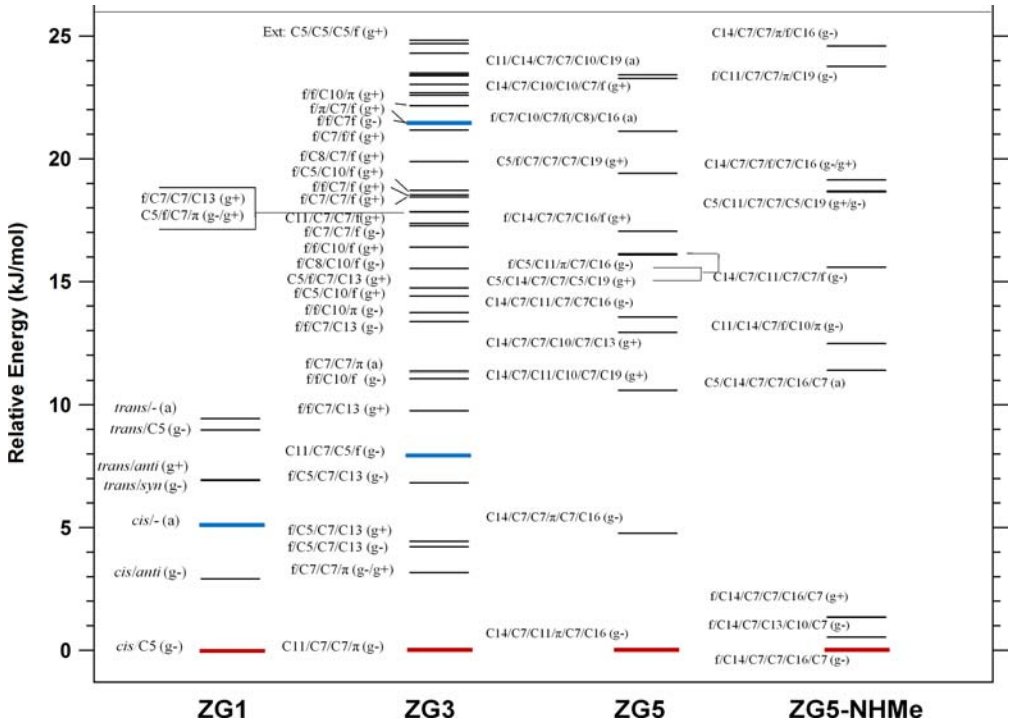


**Figure 5.** Conformational energies (zero-point corrected) within 25 kJ/mol of the respective global minima for Z-Gly-OH, Z-$(Gly)_3$-OH, Z-$(Gly)_5$-OH, and Z-$(Gly)_5$-NHMe from left to right respectively. Black lines represent the calculated energies with respect to the global minimum, with red and blue bold lines corresponding to the assigned structures (see text). Labels correspond to the H-bonding interactions of the NH/OH groups from N → C terminus.

3a,b denote the infrared frequencies used for IR−UV HB spectroscopy in Figure 2.

Parts c and d of Figure 3 present the corresponding single-conformation IR spectra of conformers A and B in the amide I/II regions. Given the extended form of conformer A of ZG1, its amide I/II spectrum also is used as reference for comparison with other structures in what follows. The amide I bands due to C═O stretch fundamentals shift to lower frequency when accepting H-bonds, with additional shifts when the NH group on the same amide is also involved in a H-bond.[54] The amide II region is associated with NH bend/CN stretch fundamentals, which shift in the opposite direction (i.e., to higher frequency) when the NH group engages in a H-bond. In this region, when NH bend modes are strongly coupled with one another in extended chains (e.g., in sequential C5 rings), the in-phase coupled bend generates a large intensity enhancement.[54,55]

In ZG1(A), the carboxylic acid CO band appears as a doublet split by 6 $cm^{-1}$ with the more intense member at 1797 $cm^{-1}$. This band is higher frequency than free amide carbonyls, and the observed splitting is likely due to a 2:1 Fermi resonance with the $(H_2)C-C(=O)$ stretch or the OH bend + C═O bend combination band, both of which are predicted to be in close proximity. The free Z-carbonyl is the intense band appearing at 1756 $cm^{-1}$. Note that the amide II transition at 1522 $cm^{-1}$ possesses an intensity nearly as large as that of its amide I counterpart. These frequencies and intensities are reproduced accurately by the calculation, shown as a stick spectrum below, further confirming this assignment. The amide I transitions of conformer B (Figure 3d) are both shifted to frequencies higher (by 9 $cm^{-1}$ and 17 $cm^{-1}$, respectively) than those of their counterparts in conformer A. These shifts are reproduced by the calculated values for the structure assigned to conformer B. In the amide II region, no band is clearly observable in the spectrum after subtraction of the conformer A spectrum, indicating that the band in the uncorrected spectrum has the exact frequency and intensity of the scaled spectrum of conformer A. As a result, we are not able to use this region in confirming the assignments. Nevertheless, the body of evidence points clearly to the structures shown in Figure 4a as those responsible for the observed spectra. The planar structure assigned to conformer A was determined to be the global minimum by the DFT M05-2X calculations, while that of ZG1(B) was 5.06 kJ/mol above that minimum.

Figure 5 displays an energy level diagram for the low-energy structures of ZG1. The black lines are zero-point corrected energies for all calculated structures within 25 kJ/mol of their respective global minimum, while the lines in bold (red and blue) are those assigned to observed conformational isomers. Since ZG1 does not have a substantial glycine chain to accommodate H-bonds, the conformational families are designated differently than in those of their larger counterparts. Two conformers of the $\beta$-strand like family are possible, depending on the NCC═O dihedral angle at the C-terminus; when a C5 is formed between the NH[1]···OC[1] it places the NH[1] and CO[1] groups *cis* to one another. When the NH[1]···OH H-bond is formed, the groups are *trans*. All other structures within 25 kJ/mol are due to the COOH coming out of the plane of the peptide backbone either *syn* or *anti* to the phenyl ring which is also perpendicular to this plane. For *anti* phenyl ring orientations, no such distinction needs to be made. This energy level diagram will be discussed in further detail in the Discussion.

**3.2. Z-$(Gly)_3$-OH (ZG3).** *3.2.1. R2PI and IR−UV HB Spectroscopy.* The R2PI and IR−UV HB spectra for ZG3 are shown in Figure 6. Only two conformers were found by IR−UV holeburning. The major conformer A has its origin

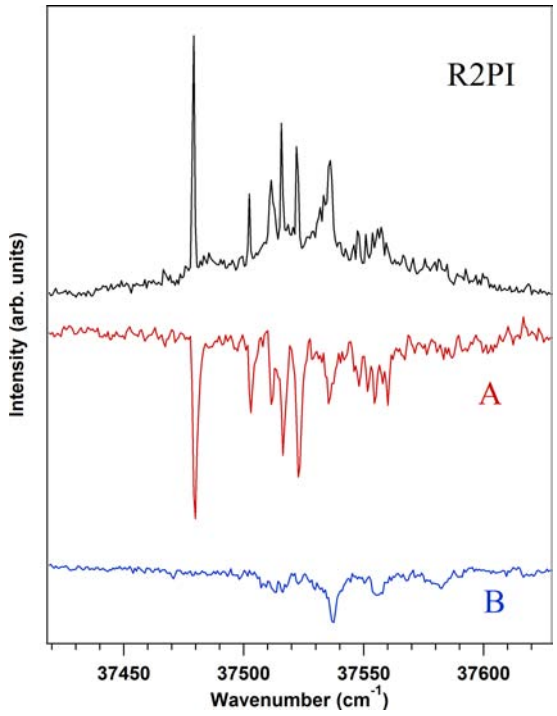


**Figure 6.** R2PI spectrum of Z-$(Gly)_3$-OH (top trace) and IR–UV HB spectra of the observed conformers (A and B). The IR transitions used for the holeburn spectra were those at 3554 and 3495 $cm^{-1}$ respectively.

transition red-shifted from ZG1(A) by 121 $cm^{-1}$, suggesting a slight perturbation to the phenyl ring by the longer glycine chain, modulating the $\pi\pi^*$ transition. A further indication of this interaction is seen in the extensive low-frequency vibronic activity for ZG3(A), with Franck–Condon active modes at 23, 32, 36, and 43 $cm^{-1}$. Their presence likely indicates the existence of a $\pi$ H-bond to the phenyl ring.

The transitions ascribed to conformer B are significantly weaker, with its $S_0$–$S_1$ origin blue-shifted by 58 $cm^{-1}$ from the ZG3(A) origin. Although not as red-shifted as conformer A, the B origin is nevertheless 63 $cm^{-1}$ to the red of the "unperturbed" ZG1 origin, again suggesting the possible presence of a weak $\pi$ H-bond.

*3.2.2. RIDIR Spectroscopy.* RIDIR spectra for conformers A and B of ZG3 are shown in Figure 7. The asterisks indicate the transitions used for IR–UV HB spectroscopy. It is immediately obvious from the hydride stretch region (Figure 7a,b) that substantial hydrogen bonding is occurring in ZG3 compared to that in ZG1. Not only are many bands shifted to much lower frequency, but several are broadened and considerably more intense, all signatures of intramolecular H-bond formation.[25,26,31,35,36,38–41,43,52,56,57]

The hydride stretch spectrum of conformer A (Figure 7a) has an OH stretch transition at 3554 $cm^{-1}$, ~30 $cm^{-1}$ below that in ZG1, indicative of a OH···$\pi$ H-bond confirmed by calculation (stick spectrum below). This interaction further explains the origin shift and vibronic activity observed in the UV spectrum. The satellite band at 3571 $cm^{-1}$ is likely a result of Fermi resonance of the OH stretch fundamental with the overtone of the COOH C=O stretch (with fundamental at 1792 $cm^{-1}$). The NH stretch fundamental at 3463 $cm^{-1}$ is close to the frequency expected for a free or nearly free NH stretch of the NH group immediately adjacent to the Z-cap. Calculations assign this band to a weak C11 H-bond to the carboxylic acid carbonyl. The two strong bands just below 3350 $cm^{-1}$ are due to NH groups in fairly strong H-bonds, appearing in a spectral region typical of C7 intramolecular H-bonded rings.[26] All of these uniquely diagnostic bands are accounted for in a C11/C7/C7/OH···$\pi$ structure. The frequency shifts between these bands are not exact, but the pattern is unequivocal in this assignment. Besides fitting the experimental spectrum well, this structure, shown in Figure 4b, was the global minimum calculated at the DFT//M05-2X/6-31+G(d) level of theory.

The amide I/II spectrum in Figure 7c for conformer A is also fit well by the calculated spectrum further confirming the assigned structure. The highest-frequency transition at 1792 $cm^{-1}$ corresponds to the COOH C=O stretch similar to ZG1. The large band at 1730 $cm^{-1}$ is the free CO[2] stretch, with a

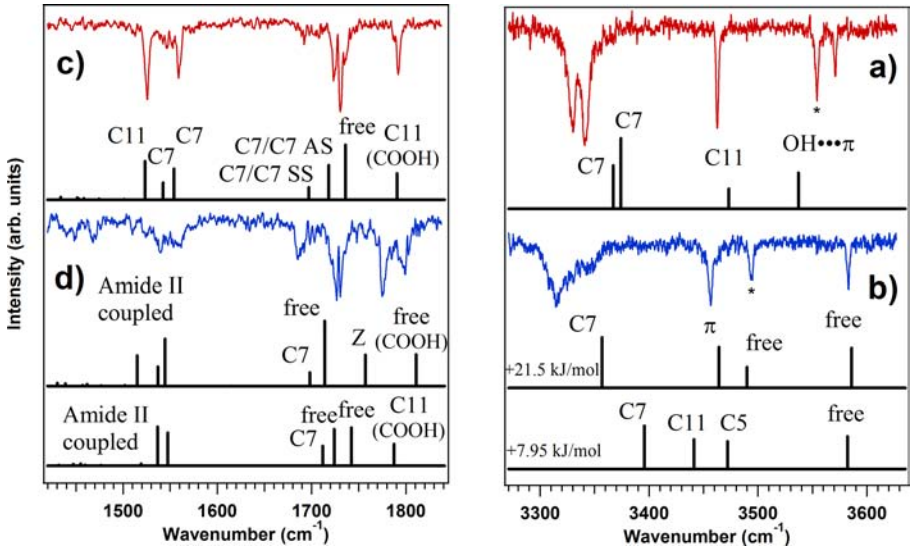


**Figure 7.** Z-$(Gly)_3$-OH amide I/II (left) and NH/OH stretch (right) RIDIR spectra for conformers A (upper) and B (lower) with calculated IR spectra calculated at the DFT//M05-2X/6-31+G(d) level of theory using scaling factors of: 0.96 (amide I/II), 0.943 (NH stretch), 0.952 (OH stretch). Asterisks indicate IR–UV holeburn transitions.


dx.doi.org/10.1021/ja306652c | J. Am. Chem. Soc. 2012, 134, 17186–17201

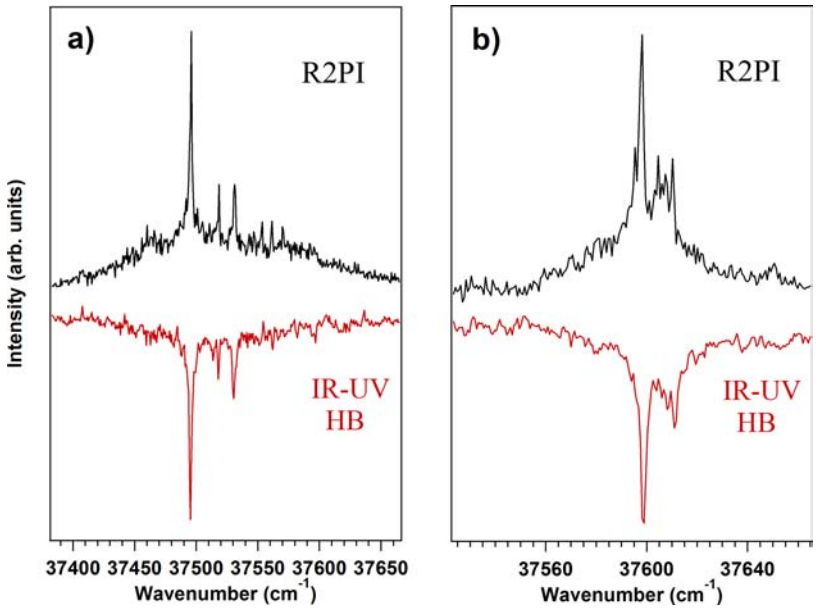


**Figure 8.** R2PI spectra (top trace) and IR−UV HB spectra (bottom trace) of (a) Z-$(Gly)_5$-OH and (b) Z-$(Gly)_5$-NHMe in the $S_0$−$S_1$ region. The IR transitions used for the holeburn spectra were those at 3350 and 3403 $cm^{-1}$, respectively.

smaller band just to the red corresponding to a coupled antisymmetric stretch mode of the two carbonyl groups accepting C7 H-bonds. The smaller band to the red in the stick spectrum is its symmetric counterpart, which is just detectable in the experimental spectrum. The agreement between experiment and calculation in the amide II region is also good, with the band at 1559 $cm^{-1}$associated with a C7 H-bond, as is the weak band just barely observable on its lower frequency edge. The intense transition at 1526 $cm^{-1}$ coincides with the weak C11 H-bond, appearing near the frequency of the free NH group in ZG1(A). These amide II spectral patterns agree with the general expectation that the amide II vibrations shift to higher frequency with increasing H-bond strength.[54]

The second conformer of ZG3 is likely to be only a small fraction of the total population, based on its weak intensity and small Franck−Condon activity in the R2PI spectrum. Conformer B has several unique aspects to its IR spectrum (Figure 7b,d) which help distinguish its structure from that of ZG3(A). Importantly, the OH stretch band at 3583 $cm^{-1}$ indicates unequivocally that the COOH group is free, a feature held by only a small fraction of the structures in Figure 5. Second, the transition at 3315 $cm^{-1}$ is even lower in frequency than the C7 bands in conformer A, indicating the presence of a strong C7 H-bonded ring. Third, the band at 3495 $cm^{-1}$ is higher in frequency than a typical free amide NH stretch, and is shifted almost 25 $cm^{-1}$ higher in frequency than the free NH groups immediately adjacent to the Z-cap in ZG1. Finally, the remaining peak at 3457 $cm^{-1}$ is only slightly lower in frequency than a typical free amide NH stretch, suggesting the potential presence of an NH···$\pi$ H-bond. If present, this would also account for the red-shifted electronic origin. Although a red-shift in the electronic origin is not general for a $\pi$ H-bond, in this case, glycine interactions with the Z-cap phenyl ring appear to lower the $S_0$−$S_1$ energy.

In the amide I region (Figure 7d), the striking difference relative to conformer A is the presence of two bands at 1775 and 1799 $cm^{-1}$ in B, while only one is present in this region in ZG3(A). The two groups capable of possessing such high-frequency C═O stretch bands are the COOH and Z-cap C═O groups (the latter a part of an ester). By virtue of their frequencies, both these groups are free or nearly free of H-bonding interactions. In particular, the COOH group is essentially in the same environment as ZG1(A) with the C-terminal residue taking on a planar configuration. This is verified by the C═O stretch band at 1799 $cm^{-1}$ compared with the ZG1(A) band at 1797 $cm^{-1}$. The band at 1775 $cm^{-1}$ is predicted to be the Z-cap C═O stretch by calculation, but the calculations do not reproduce the frequency shift accurately. However, the experimental frequency of this band is very close to the Z-C═O stretch fundamental in ZG1(B) (Figure 3d). The intense amide I transitions at 1727 $cm^{-1}$ and its weak partner at 1685 $cm^{-1}$ are in the regions where typical free amide I vibrations and C7 H-bonded rings appear, respectively. Finally, the amide II region of the ZG3(B) spectrum has a broad absorption with less-defined structure compared to that in conformer A.

When taken as a whole, the constraints placed on the structure of conformer B by the NH/OH stretch and amide I regions removes from consideration most of the low-energy structures of ZG3. The best match with experiment in both the NH stretch and amide I regions is the f/$\pi$/C7/f(g+) structure, with calculated spectrum shown as a stick diagram immediately below the experiment in Figure 7b,d. This structure has the free COOH OH group, accounting for the band at 3583 $cm^{-1}$. The shift to lower frequency of the lowest-frequency NH stretch (3315 $cm^{-1}$) relative to conformer A is also predicted well by the calculation for this structure. We attribute the drop in frequency to the fact that the NH[3] group is involved in two H-bonds, principally with the CO[1] in a C7 ring, and with CO[3] in a C5 ring with the planar, terminal residue. This bifurcated double ring structure may contribute to the additional broadening observed for this band. The unusually high frequency of the free NH stretch transition at 3495 $cm^{-1}$ is also captured in large measure by the calculation, since NH[1] does not have a weak C5 interaction, like it does in ZG1(A), and also possesses an unusual configuration in which the neighboring NH[2] group is eclipsed with the CN[1] axis,


dx.doi.org/10.1021/ja306652c | J. Am. Chem. Soc. 2012, 134, 17186−17201

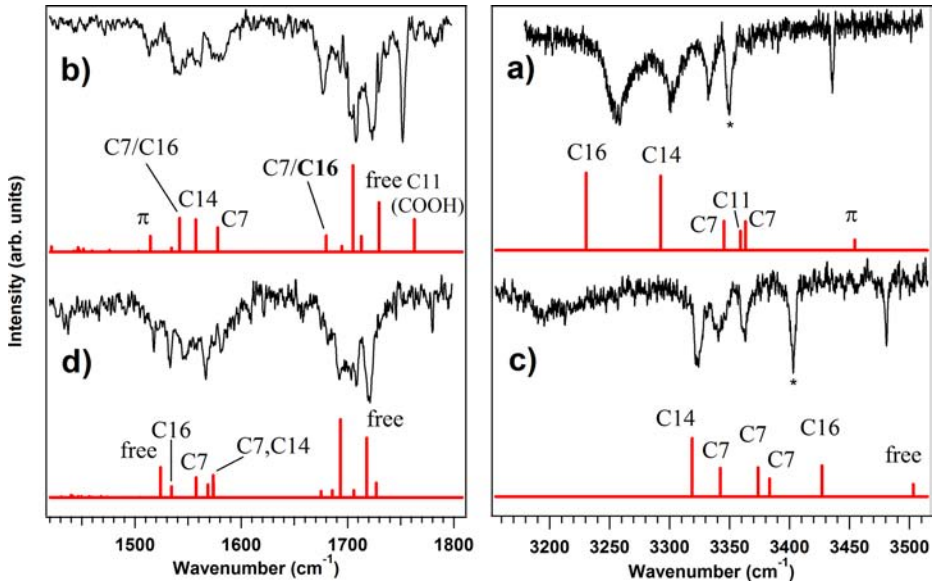


**Figure 9.** Amides I/II (left) and NH/OH stretch (right) RIDIR spectra for Z-$(Gly)_5$-OH (upper) and Z-$(Gly)_5$-NHMe (lower) with calculated IR spectra calculated at the DFT//M05-2X/6-31+G(d) level of theory using scaling factors of: 0.96 (amide I/II), 0.943 (NH stretch), 0.952 (OH stretch). Asterisks indicate IR−UV holeburn transitions.

which appears to shift the NH[1] stretch to still higher frequency.

In the amide I region, this structure has both Z-C═O and COOH groups free, thereby accounting for the two high-frequency amide I transitions at 1775 and 1799 $cm^{-1}$. The large band centered at 1727 $cm^{-1}$ is assigned to the free amide CO[2]. The splitting of this peak in the experimental spectrum is artificial, arising from a dip in IR power caused by a large water transition that is present due to insufficient purging of the IR beam path during the acquisition of this spectrum. The smaller transition to the red of this band is the C7 carbonyl acceptor fundamental.

Finally, the calculation reveals that the amide II modes are coupled between all three NH groups, unlike the spectrum of conformer A where this region consisted of NH bends that were highly localized on a single NH group. It is hypothesized that this coupling may play a role in inducing the broadening observed.

The striking result of the assignment of conformer B to an f/$\pi$/C7/f(g+) structure is that this structure possesses only one strong H-bond and has a calculated energy 21.5 kJ/mol higher than the global minimum structure assigned to conformer A. As Figure 5 shows, many minima exist between these two conformers on the potential energy surface which are not observed. Due to this fact, we have carefully considered other possibilities. Of them, the C11/C7/C5/f(g−) structure with calculated energy of +7.9 kJ/mol was the next best alternative. While it captures the general pattern in the NH stretch region, the C7 NH stretch is predicted to be higher in frequency than those in conformer A, at odds with experiment. In the amide I region, this structure places the Z−C═O group in a C7 H-bond, and so does not reproduce very well the two high-frequency C═O stretch bands observed experimentally. In the amide II, its fit to experiment is arguably better than the f/$\pi$/C7/f(g+) structure.

In summary, the unusual spectrum of conformer B of ZG3 is best accounted for by the f/$\pi$/C7/f(g+) structure, but its high energy lends some uncertainty to the assignment. Some possible reasons for its presence in the expansion are posed in the Discussion. However, no matter what the ultimate resolution is, conformer B is at most a minor conformer, one of only two observed in the spectrum, which is dominated by the C11/C7/C7/$\pi$(g−) conformer that is calculated to be the global minimum on the potential energy surface.

**3.3. Z-$(Gly)_5$-OH (ZG5) and Z-$(Gly)_5$-NHMe (ZG5-NHMe).** *3.3.1. R2PI and IR−UV HB Spectroscopy.* The R2PI and IR−UV HB spectra for ZG5 and ZG5-NHMe are shown in Figure 8. The R2PI and IR−UV HB spectra for both ZG5 and ZG5-NHMe are essentially identical confirming the existence of only one conformer in the jet for both molecules. This is a striking result. Despite the substantially greater flexibility accompanying the increase in glycine chain length, all of the population resides in a single minimum in both cases. The $S_0$−$S_1$ origin in ZG5 is 105 $cm^{-1}$ red-shifted from ZG1, at 37496 $cm^{-1}$, near that of both ZG3 conformers, which proved to be indicative of a $\pi$ H-bond. In contrast, ZG5-NHMe shows an origin transition only 3 $cm^{-1}$ to the red of the ZG1(A) origin, suggesting that the phenyl ring is isolated from interactions with the peptide chain. Two small vibronic bands in ZG5 were observed at +23 and +35 $cm^{-1}$ above the origin.

*3.3.2. RIDIR Spectroscopy.* The RIDIR spectra for ZG5 are shown in Figure 9a,b, and those of ZG5-NHMe in Figure 9c,d. As with ZG1 and ZG3, all structures calculated by DFT M05-2X were compared with the experimental spectra in the assignment process. For both molecules, there are six XH oscillators whose fundamentals should appear in the IR spectrum, five NH and one OH for ZG5, and six NH for ZG5-NHMe. While Figure 9 presents only the best fit results, the spectrum for ZG5-NHMe is compared with the three lowest-energy structures in the Supporting Information (Figure S2).

In ZG5 (Figure 9a), the highest-frequency band observed is at 3435 $cm^{-1}$, which is shifted well below the free NH stretch region (37 $cm^{-1}$ red of ZG1(A)). The region from 3510 to 3600 $cm^{-1}$ (not shown) was also scanned, showing no absorption ascribable to a free COOH OH stretch. This is immediate evidence that every NH/OH group in this conformation is involved in a H-bond. The two transitions at


dx.doi.org/10.1021/ja306652c | J. Am. Chem. Soc. 2012, 134, 17186−17201

3350 and 3332 $cm^{-1}$ fall in the spectral region anticipated for C7 H-bonded rings (see the spectrum of ZG3 in Figure 7). The broadened band at 3301 $cm^{-1}$ is shifted below the typical C7 range, and the large transition centered at 3258 $cm^{-1}$ is significantly broadened with a fwhm of ~18 $cm^{-1}$. The features of these two transitions are suggestive of especially strong H-bonds, and the band at 3258 $cm^{-1}$ is characteristic of a strong carboxylic acid H-bond based on previous studies.[57,58]

The stick diagram in Figure 9a contains the spectrum that matches the experimental data best. The structure associated with this spectrum is shown in Figure 10a, which is also the global minimum among all calculated structures (Figure 5). It is a compact, tightly folded structure that maximizes the number and strength of H-bonds present, which according to our labeling scheme is C14/C7/C11/$\pi$/C7/C16(g−). The stick spectrum assigns the band at 3435 $cm^{-1}$ as an NH···$\pi$ H-bond. Its presence also explains the red-shift in $S_0-S_1$ origin frequency relative to ZG1(A). The transitions in the C7 frequency regime are indeed C7 H-bonds, with a fundamental due to a C11 H-bonded ring at nearly the same frequency as one of the C7 fundamentals. We hypothesize on this basis that the band at 3350 $cm^{-1}$ is an unresolved doublet, whose larger intensity arises from that fact. The broadened peak near 3300 $cm^{-1}$ is accounted for as a strong C14 H-bonded ring, while the intense, broadened transition at 3258 $cm^{-1}$ involves the carboxylic acid OH in a close H-bond to CO[1], making a large C16 intramolecular ring.

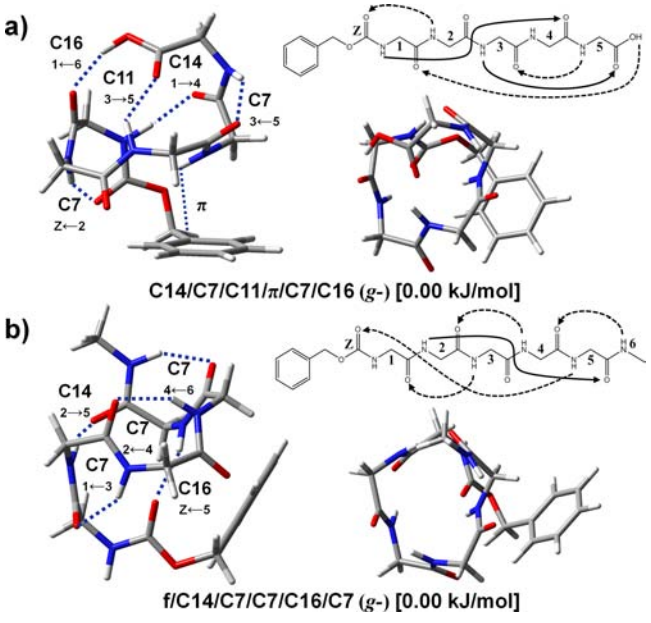


**Figure 10.** Assigned C14/C16 mixed helix structures for (a) Z-$(Gly)_5$-OH and (b) Z-$(Gly)_5$-NHMe showing the H-bonding patterns of each with labels. The top view and schematic representation of H-bonding patterns are shown to the right of each labeled structure. Structures were calculated using DFT at the M05-2X/6-31G+(d) level of theory.

The close comparison between experiment and calculation in the amide I/II region (Figure 9b) confirms and strengthens this assignment. The lack of any transitions above 1760 $cm^{-1}$ confirms that both the Z and COOH carbonyls are in H-bonds. The highest-frequency transition at 1752 $cm^{-1}$ is due to the COOH CO, which acts as acceptor in a C11 H-bonded ring. The intense band at 1723 $cm^{-1}$ arises from the free CO[2], similar to ZG3(A), while the set of bands near 1708 $cm^{-1}$ are a highly coupled set involving motion of CO[Z], CO[1], CO[3], and CO[4] carbonyls which are acceptors in C7, C16, C7, and C14 H-bonded rings respectively. The lowest-frequency transition at 1677 $cm^{-1}$ is a primarily uncoupled CO[1] stretch involved in the strong C16 H-bond. This trend agrees with the expected correlation of H-bond strength with red-shift in amide I frequency.

The amide II region shows smaller, broader absorptions, but even here the stick spectrum reproduces the features fairly well. According to the calculations, these bands are largely localized on single amide groups, as labeled in the stick diagram.

The C14/C7/C11/$\pi$/C7/C16(g−) structure is shown both from side and top views in Figure 10a along with a schematic representation of the H-bonding scheme. It comprises approximately one-and-a-half turns of a helix that is held together by three long-range H-bonds (C11, C14, and C16), supplemented by nearest-neighbor C7 rings that bend the backbone along the helical path and further stabilize the structure. The dihedral angles for this structure can be found in Table 1. Interestingly, while the C11 and C14 H-bonds are directed from N → C terminus, the C7 and C16 H-bonds point in the reverse direction (C → N). For this reason, in what follows, we will refer to this structure as a C14/C16 helix.

A close look at the structure shown in Figure 10a makes clear that the carboxylic acid at the C-terminus plays a key role in holding together and terminating the helix. This raises the question whether the mixed helix formation would remain if the COOH group was modified to better represent a pentaglycine subunit in a longer polypeptide. To address this, ZG5 was

**Table 1. Relative Energies and Ramachandran Angles for the Assigned Structures in All Z-$(Gly)_n$ Molecules**

| | ΔE (kJ/mol) | $\varphi_1$(°) | $\psi_1$(°) | $\varphi_2$(°) | $\psi_2$(°) | $\varphi_3$(°) | $\psi_3$(°) | $\varphi_4$(°) | $\psi_4$(°) | $\varphi_5$(°) | $\psi_5$(°) | $C_\varphi C_\alpha OC$ |
|---|---|---|---|---|---|---|---|---|---|---|---|---|
| ZG1 A | 0.00 | 179.1 | 179.8 | - | - | - | - | - | - | - | - | -84.2 (g-) |
| ZG1 B | 5.06 | 72.62 | -174 | - | - | - | - | - | - | - | - | -174 (a) |
| ZG3 A | 0.00 | 77.47 | -76.08 | -79.69 | 80 | 67.8 | -164.4 | - | - | - | - | -97.8 (g-) |
| ZG3 B | 21.5 | -84.51 | 12.37 | -83.94 | 59.72 | 178.7 | -179.3 | - | - | - | - | 68.7(g+) |
| ZG5-OH | 0.00 | 81.26 | -64.76 | -92.91 | 55.53 | 140 | -40 | -80.82 | 81.71 | 61.62 | -141.4 | -93.4 (g-) |
| ZG5-NHMe | 0.00 | -52.08 | 136 | 80.82 | -57.41 | -81.03 | 69.61 | 98.8 | -36.36 | -85.15 | 79.19 | -69.1 (g-) |


dx.doi.org/10.1021/ja306652c | J. Am. Chem. Soc. 2012, 134, 17186−17201

capped with −NHMe at the C-terminus, and studied by the same methods.

The RIDIR spectrum for ZG5-NHMe in the NH stretch region is shown in Figure 9c. Once again, the calculated best-fit spectrum is shown as a stick diagram immediately below the experimental spectrum. In ZG5-NHMe, the highest-frequency transition appears at 3481 $cm^{-1}$, shifted up in frequency from the ZG1(A) NH by 9 $cm^{-1}$. This transition is then a signature of a free NH stretch of NH[1], immediately adjacent to the Z-cap, and provides an important constraint to the structural search. The transition at 3403 $cm^{-1}$ is associated with a weak C16 ring that links NH[5] → CO[Z], and is quite different from the C16 ring in ZG5 that involved the carboxylic acid OH group. The bands at 3363 and 3341 $cm^{-1}$ are reasonably assigned as C7 interactions. According to the calculations, three transitions appear in this region, and we hypothesize that the more intense of the two experimentally (3363 $cm^{-1}$) is an unresolved doublet due to the two higher frequency sticks. The band centered at 3323 $cm^{-1}$ is shifted to slightly higher frequency than the strong C7 NH stretch observed in ZG3(B), but is fairly close to the C14 band in ZG5. Indeed, it is assignable as a C14 ring joining the NH[2] → CO[5] groups. Finally, the broad, weak transition near 3190 $cm^{-1}$ (Figure 9c) is too low in frequency to be an amide NH stretch fundamental. Of the 70 lowest-energy calculated structures for ZG5-NHMe, none have a scaled NH stretch fundamental below 3275 $cm^{-1}$. This is in keeping with the fact that the lowest-frequency band in the spectrum of ZG5 (Figure 9a) is associated with the OH group, which is not present in ZG5-NHMe. Instead, we tentatively assign the broad band near 3190 $cm^{-1}$ in ZG5-NHMe as an overlapping set of amide I/amide II combination bands (1500 + 1700 $cm^{-1}$), with a width similar to that of the amide II fundamental (Figure 9d).

The amide I/II spectrum for ZG5-NHMe in Figure 9d is not as well-resolved as its ZG5 counterpart (Figure 9b). The additional broadening in this spectrum is likely due to saturation effects necessary to achieve the depletion signal for the acquisition of the spectrum. Nevertheless, the spectrum confirms the assignment made based on the amide NH stretch region. First, no COOH C═O stretch exists in this molecule so the highest-frequency band in the spectrum is found at 1721 $cm^{-1}$, close to the position of the free CO stretch in Figure 9b. The calculated spectrum predicts the presence of a smaller band on the high-frequency side of this peak, corresponding to the CO[Z] stretch in the C16 H-bond, which is not clearly resolved in the experimental spectrum. The congested clump of transitions centered around 1700 $cm^{-1}$ is calculated to be the result of a set of coupled oscillators due to CO[2](C7)/CO[4](C7)/CO[5](C14) groups. The amide II region has a different absorption profile with sharp structure on top of a broad absorption that may arise at least in part from saturation effects. As a result, it is difficult to use this region in detail for assignment purposes. However, many of the sharp features observed do coincide with the calculated results for the assigned structure, and the corresponding amide groups responsible for these bands are displayed above the stick spectrum.

The conformation of ZG5-NHMe responsible for the observed spectrum is shown in Figure 10b. This structure incorporates many of the same H-bonding interactions as in ZG5 despite the substitution of NHMe for OH; notably including a C14/C16, $i \rightarrow (i+3)/i \leftarrow (i+5)$ motif with nearest-neighbor C7 rings contributing to the turns in the helix. As in ZG5, this structure shows the first stages of formation of a C14/C16 helix, even when the strong COOH OH H-bond is removed as a stabilizing factor. Not surprisingly, the groups used for forming C14 and C16 H-bonds differ in ZG5 and ZG5-NHMe, and in fact, the OH group forms the C16 H-bond in ZG5. At the same time, upon closer inspection, ZG5 and ZG5-NHMe show marked similarities in backbone structure between amide group '*i*' in ZG5 and '*i* + 1' in ZG5-NHMe that will be discussed in more detail in the Discussion. The designation of this structure from N → C terminus is f/C14/C7/C7/C16/C7(g−). Once again, it is the global minimum among the DFT optimized structures as illustrated in Figure 5. Further support of this assignment lies in the frequency of the electronic origin which is found very near the ZG1 frequency since no perturbation to the phenyl ring is predicted. These results demonstrate that a mixed helix conformation is the global conformational preference for these Z-capped polyglycine chains five residues long in the absence of solvent.

## 4. DISCUSSION

Conformation-specific IR spectra in the NH/OH stretch and amide I/II regions have been used to determine the conformational preferences of ZG1, ZG3, ZG5, and ZG5-NHMe under isolated-molecule conditions in the gas phase. As Figure 5 shows in pictorial form, in every case, the conformation dominating the observed spectrum is also calculated to be the global minimum, lending some confidence that the DFT M05-2X/6-31+G(d) calculations are correctly ordering the relative energies of the minima. This is in notable contrast to other cases where the relative free energies of the conformers at the pre-expansion temperature rather than enthalpic terms dictate the observed conformer population.[59,60] In this case, the enthalpic preferences are strong enough not to be undone by differences in entropy, and may be a unique feature of the polyglycines. Free energy corrections are provided in the Supporting Information (Table S2). Nevertheless, the case of ZG3 in supporting a second conformer which is high in energy indicates that other aspects of the potential energy landscapes beyond the global minimum are important. In what follows, we turn attention first to a discussion of these potential energy landscapes.

**4.1. Potential Energy Landscapes for Z-(Gly)$_n$-OH, $n$ = 1, 3, 5 and Z-(Gly)$_5$-NHMe.** One of the most striking results of the present study is the small number of conformations observed for each molecule, with ZG1 and ZG3 spreading their population over two conformers, while both ZG5 and ZG5-NHMe have measurable population in a single conformational minimum. Given the high degree of flexibility inherent to the glycine residues, one might have anticipated a sharp increase in the number of low-lying conformational minima with increasing size '*n*'. In direct contrast to this notion, Figure 5 predicts clearly that the number of conformational minima with energies within 25 kJ/mol of the global minimum is distinctly nonmonotonic with increasing size '*n*', displaying a sharp increase in going from $n$ = 1−3, but then a dramatic reduction in the number of low-lying minima in both ZG5 and ZG5-NHMe. In fact, within the first 10 kJ/mol (equivalent to 4 kT at room temperature), there are only two conformational minima predicted for ZG5 and three for ZG5-NHMe. This result indicates that the network of H-bonds present in the low-energy pentaglycine structures provide unique stability.

The ZG1 molecule is too short to form significant intramolecular H-bonds. As a consequence, the global

minimum structure and dominant conformer observed is an extended conformation with a weak C5 H-bond as the only such interaction. The other types of conformations shown in Figure 5 come from structures that orient the COOH group out of the C(O)−N(H)−C($\alpha$) plane. Within this family of structures, *cis* or *trans* configurations of the out-of-plane COOH C═O relative to the amide N are possible, and the bent COOH orients either *syn* or *anti* to the phenyl ring in *gauche* ring configurations. There is no orientational designation for *anti* ring orientation since in this case the *syn*/*anti* COOH configurations become equivalent. The *cis*/-(a) structure was also observed in the experiment, which is the second lowest-lying minimum above the global minimum. The structure about 9 kJ/mol above the global minimum is the *trans* equivalent to the observed *cis* extended structure, with a C5 ring present between NH···OH.

With the addition of two more glycine residues in forming ZG3, the molecule gains sufficient flexibility to begin forming multiple H-bonds that fold the molecule into well-defined conformational families. This is immediately apparent from the labeling scheme used in Figure 5. Not surprisingly, there is a clear correlation between the energy stability and the number of intramolecular H-bonds present. In particular, the global minimum incorporates back-to-back C7 nearest-neighbor H-bonds that turn the backbone optimally so that the COOH group can form additional C11 and $\pi$ H-bonds. Conformational families going up in energy then nominally either lose H-bonds or are replaced by weaker H-bonds (e.g., C5 for C7).

In light of the general correlation between number of H-bonds and energetic stability, the presence in ZG3 of a minor conformer (conformer B) tentatively assigned to a structure that contains only a C7 and $\pi$ H-bonds, with an energy 21.5 kJ/mol above the global minimum, is decidedly unexpected. In fact, if the assignment is correct, its presence in the face of the multitude of structures with lower energy that are not observed (Figure 5), presents an unresolved issue begging to be answered. Unfortunately, we have no unequivocal answer, and can only suggest a few possibilities. First, the populations observed downstream in the expansion are influenced both by the conformational space sampled by the molecules in the laser desorption plume, plus the kinetic competition for trapping during the collisional cooling process that immediately follows. If we assume, for the sake of argument, that the initial conformational distribution is thermally equilibrated at an initial desorption temperature of 300 K, then the initial relative populations are determined by the relative free energies at this temperature. Extended structures are lower in free energy because their floppy nature belies a greater number of low-frequency vibrational modes. Table S2 in the Supporting Information lists both the zero-point corrected energies and the 300 K free energies of the conformers within 50 kJ/mol of the global energy minimum of ZG3. It is noteworthy that the free energy of the structure assigned to conformer B at 300 K is only 4.5 kJ/mol above that of A, a drop of almost 17 kJ/mol relative to its zero-point corrected energy difference. Thus, it is at least plausible that this structure has population in it prior to cooling. Similar results have explained the anomalous existence of energetically high-lying extended conformers in other studies.[59,60] Second, the extended structures also gain population as a class of structures by virtue of their great number. Thus, additional population could get funneled during the cooling process into conformer B from the other extended conformers, if the barriers separating them are comparatively small. Third, in order for this scenario to account for observation, it would necessitate the presence of comparatively large barrier(s) separating some subset of the extended structures from the folded conformers that lead to conformer A. Indeed, the global free energy minimum is predicted to be due to a fully extended structure with energy 8.4 kJ/mol below that of the C11/C7/C7/$\pi$ structure assigned to conformer A. This structure and others like it would need to partially fold into conformer B in early stages of cooling before being trapped there behind a large barrier. This calls for a much more comprehensive knowledge of the potential energy surface than we have at present, and argues for further theoretical investigation. It would be very instructive to generate disconnectivity diagrams[61,62] for the ZGly series. This is a pathway we are presently pursuing.

In ZG5, the single observed conformation is the global minimum, forming the beginning stages of a C14/C16 helix (C14/C7/C11/$\pi$/C7/C16(g−)). The one other structure calculated to be within the first 10 kJ/mol appears 5 kJ/mol above the global minimum, but also retains the C14/C16 motif, differing from the global minimum only by flipping the COOH by 180°, thereby replacing the C11 ring by a nearest-neighbor C7 interaction. At energies higher than 11 kJ/mol, the C14/C16 combinations are lost, with other H-bonding motifs taking their place. In forming this structure, ZG5 has all its groups tied up in H-bonds, including NH[4], which engages in a $\pi$ H-bond with the phenyl ring. The global minimum for ZG5-NHMe is also an incipient C14/C16 helix (f/C14/C7/C7/C16/C7-(g−)), but in this case two other minima appear within 2 kJ/mol of the global minimum. These structures differ only subtly from the global minimum. In the second most stable structure, the NH[4] and NH[5] groups swap H-bond partners (NH[4]···OC[2]/NH[5]···OC[Z] → NH[4]···OC[Z]/NH[5]···OC[2]). The spectral patterns associated with this swap are clearly a poorer fit to experiment, ruling it out as the experimentally observed structure. Furthermore, the structure next higher in energy (at 1.35 kJ/mol) has an identical peptide backbone to the global minimum, but with a different phenyl ring orientation (g+ rather than g−). The simulated IR spectra for these two structures are very similar, and cannot be differentiated unequivocally by comparison with experiment. Since both share the same peptide backbone structure, conclusions drawn on that basis are not changed. This comparison is included in the Supporting Information.

One might wonder about the effect of the Z-cap on the observed preference of ZG5 and ZG5-NHMe for C14/C16 mixed helices. As we have just mentioned in ZG5, NH[4] engages in a $\pi$ H-bond with the Z-cap phenyl ring. While this interaction with the Z-cap undoubtedly adds stability to the structure, its contribution is small compared to the amide−amide and COOH/amide H-bonds. Furthermore, in ZG5-NHMe, a similar mixed helix backbone structure is formed even in the absence of the $\pi$-bond, confirming that the interactions with the Z-cap are not large, and are not likely to be responsible for mixed helix formation, but rather are formed as a natural byproduct, when possible, adding slightly greater stability to the mixed helix.

Interestingly, the magnitudes of the free energy corrections in ZG5-NHMe are far smaller than those in ZG3, and in fact favor the global minimum relative to the next two structures just discussed, which are 4.1 and 6.7 kJ/mol higher in free energy. In summary, the most stable conformations of both pentaglycines are aptly characterized as C14/C16 helices

regardless of the nature of the C-terminal cap, and the enhanced stabilization gained by forming the initial stages of this unique secondary structure places it well below the energies of other conformations on the potential energy surfaces for the two molecules.

**4.2. $H_{14/16}$ Mixed Helices.** The dominant preference in both pentaglycines ZG5 and ZG5-NHMe for a structure that shows the first stages of formation of a C14/C16 helix provides direct experimental verification of the computational predictions of Baldauf et al. on model $H_{14/16}$ mixed helices.[15] In their calculations on capped glycine hexamer, the $H_{14/16}$ mixed helix is characterized by Ramachandran angles alternating in sign, and was found to be significantly more stable than its periodic $3_{10}$ analogue helix either in isolated form or in a low dielectric medium.[15] In comparing the experimentally discovered ZG5 conformations with the glycine hexamer used in those previous calculations, the alternating $\varphi/\psi$ dihedral angles, signature C14/C16 $i \rightarrow (i+3)/i \leftarrow (i+5)$ H-bonds, and small dipole moment that accompany the mixed helix secondary structure are all present in the observed C14/C16 helical structures. The Ramachandran angles for the amino acid residues in these two structures are plotted in Figure 11 on a standard glycine

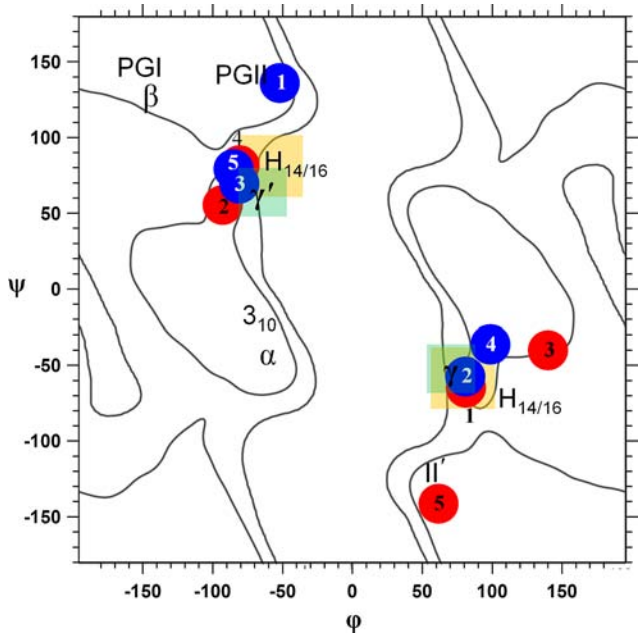


**Figure 11.** Ramachandran plot showing the $\varphi/\psi$ dihedral angles for common backbone conformations. The contours outline regions of common glycine-containing proteins, and was taken from Read et al.[3] (Reprinted, with permission from Elsevier, from *Structure* **2011**, *19*, 1395−1412; Copyright 2011.) The dots are the $\varphi/\psi$ angles for ZG5-OH (red) and ZG5-NHMe (blue) C14/C16 helices observed.

Ramachandran plot taken from Read et al. based on protein data bank X-ray crystallographic data.[3] In Figure 11, the Ramachandran angles for ZG5 and ZG5-NHMe are also compared with common periodic secondary structures and with the $H_{14/16}$ helix from Baldauf et al.[15,16] The red dots in Figure 11 denote the sets of angles associated with ZG5, while the blue dots are those for ZG5-NHMe. Within each molecule, the alternating nature of the dihedral angles is seen by the near-symmetry about the symmetry axis along the off-diagonal of the plot. It is clear that the experimental angles fall squarely into the region of the $H_{14/16}$ helix (represented nominally by orange boxes), even for residues that are not themselves directly involved in C14 or C16 hydrogen bonds. They also fall near the $\gamma$−turn region (labeled with green boxes) which is characteristic of the C7 H-bonded rings which pivot the helix backbone. In this sense, the beginnings of the $H_{14/16}$ helix appear already in a pentapeptide, since little backbone rearrangement is needed to turn C7 rings into C14/C16 H-bonds that reach across to amide groups in the next helical turn. The unique stability of the observed C14/C16 helical structures in ZG5 and ZG5-NHMe (Figure 5) arises from the fact that these structures maximize the number of intramolecular H-bonds, but do so without inducing a long-range charge separation in the molecule.

*4.2.1. Effects of C-Terminus Capping: Comparing ZG5-OH and ZG5-NHMe.* Although it may not be immediately evident from the structures shown in Figure 10, the ZG5-OH and ZG5-NHMe structures are closely similar in their backbone conformation. In order to highlight this fact, Figure 12 presents

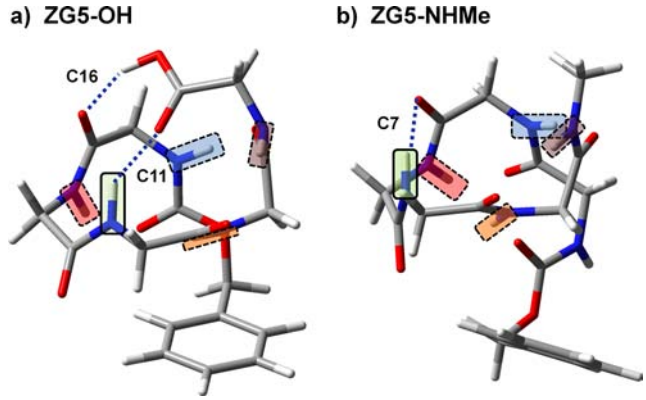


**Figure 12.** Structures for ZG5-OH and ZG5-NHMe with color-coded −NH groups demonstrating the similarity in structures (as proven by $\varphi/\psi$ angles shown in Table 1). The correspondence goes as $i:j+1$ between ZG5-OH:ZG5-NHMe; the dashed boxes indicate groups on residues with nearly identical dihedral angles whereas the solid box at $i:j+1 = 3:4$ shows the difference imposed by the −COOH on ZG5-OH due to the strong COOH bridge.

alternative views of the two structures with corresponding NH groups shaded in the same color to visualize the correspondence, which is made between amide group '*i*' in ZG5-OH and amide '*i* + 1' in ZG5-NHMe. With this shift, the COOH group in ZG5-OH extends the helix by forming a bridge via C16 and C11 H-bonds (Figure 12a) that replaces a nearest-neighbor C7 H-bond in ZG5-NHMe (Figure 12b). The similarities between amide groups '*i*' and '*i* + 1' are also readily apparent in Table 1 (colored outlines), where the Ramachandran angles are listed. These values are strikingly similar all along the peptide backbone, apart from $\varphi(3) \leftrightarrow \varphi(4)$, where ZG5-OH opens up to break the C7 H-bond present in ZG5-NHMe in forming the C11/C16 COOH bridge. This structural similarity is somewhat surprising given the significant differences in the IR spectra of the ZG5-OH and ZG5-NHMe conformers (Figure 9a,c). However, the most striking difference is in the C16(OH) fundamental near 3250 $cm^{-1}$ in ZG5, which is absent in ZG5-NHMe. The large shift in the OH stretch fundamental in forming the C16 ring involving the COOH group indicates that in ZG5, the COOH group is strongly bound to the peptide backbone in forming the C16/C11 bridge (Figure 12a). The short H-bond distance (1.80 Å) for the OH···O═C C16 H-


dx.doi.org/10.1021/ja306652c | *J. Am. Chem. Soc.* 2012, 134, 17186−17201

**Table 2. Hydrogen Bonding Distances for all Assigned Z-(Gly)$_n$ Structures Calculated at the M05-2X/6-31G+(d) Level of Theory Designated by NH/OH Number**

| conformer/XH # | 1 (Å) | 2 (Å) | 3 (Å) | 4 (Å) | 5 (Å) | 6 (Å) |
|---|---|---|---|---|---|---|
| ZG1(A) | 2.29 (C5) | f | – | – | – | – |
| ZG1(B) | 2.92 (C5) | f | – | – | – | – |
| ZG3(A) | 2.57 (C11) | 2.04 (C7) | 2.05 (C7) | ~2.80 ($\pi$) | – | – |
| ZG3(B) | f | ~ 3.01 ($\pi$) | 2.10 (C7) | f | – | – |
| ZG5-OH | 1.88 (C14) | 1.96 (C7) | 1.99 (C11) | ~2.82 ($\pi$) | 2.13 (C7) | 1.80 (C16) |
| ZG5-NHMe | f | 1.94 (C14) | 2.00 (C7) | 1.98 (C7) | 1.98 (C16) | 2.11 (C7) |

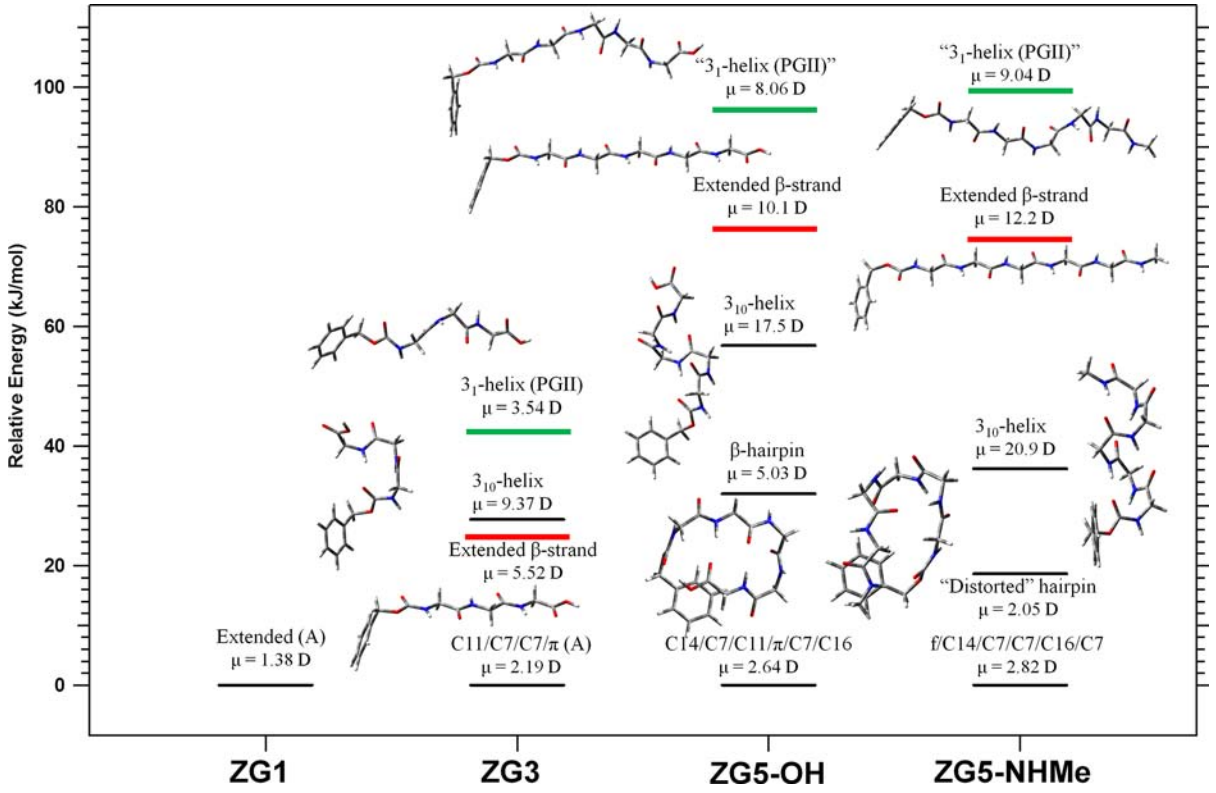


**Figure 13.** Energy level diagram comparing the observed structures with common secondary structures calculated at the same level of theory (M05-2X/6-31G+(d)). The black lines represent zero-point corrected energies for the respective conformational minima, green lines are highlighting the common condensed-phase polyglycine 3$_1$-helix (PGII), and red lines are structures that did not converge to a minimum but are transition states in the lowest-frequency mode.

bond is evident in Table 2, which accounts for the large shift in its frequency.

In ZG5-NHMe, the C16 H-bond is formed between two amide groups across an NH[5]···Z(O═C) H-bond that has a H-bond distance of 1.98 Å (Table 2). The much weaker H-bond appears at 3403 cm$^{-1}$, in a gap where no corresponding absorptions appear in ZG5. In between, the set of closely spaced transitions between 3300 and 3350 cm$^{-1}$ are indeed similar between the two structures (Figure 9a,c), with C7 H-bonds near 3350 cm$^{-1}$.

Finally, it is worth noting that the beginning stages of mixed helix formation are already evident from a comparison of ZG1(A) and ZG3(A) with ZG5-OH. While ZG1(A) is so short as to take on a shape dictated largely by the Z-capping group, it nevertheless shares the same Z-cap orientation (g-) as ZG3(A) and ZG5-OH. ZG3(A) has a peptide backbone that just forms a first full turn of the helix, with ZG5-OH sharing the same structure over the first full turn in extending the helix to 1.5 turns. As Table 1 shows, the Ramachandran angles for the first two amide groups of ZG3 and ZG5 are similar to one another, consistent with an overlap between their peptide backbones. An overlay of ZG1(A), ZG3(A), and ZG5 structures can be found in the Supporting Information, demonstrating this result.

*2. Comparing C14/C16 Mixed Helices with Common Secondary Structures.* A primary goal of the present study was to ascertain the inherent conformational preferences of a sequence of homoglycine peptides in the gas phase, where solvent effects and peptide−peptide interactions that dominate condensed phase environments are no longer present. Not surprisingly, the prototypical polyglycine structures present in these environments (PGI and PGII) are not represented in the observed conformers, in large measure because these structures depend for much of their stabilization on intermolecular H-bonds. The observed structure for ZG5-OH and ZG5-NHMe are both compact, "mixed helix" structures containing five amide−amide H-bonds. The long-range C14/C16 $i \rightarrow (i + 3)/i \leftarrow (i + 5)$ H-bonds reduce the magnitude of the dipole moment due to the opposing directions along the peptide backbone (N-terminal → C-terminal and C-terminal → N-terminal) and nearly antiparallel orientations. The nearest-


dx.doi.org/10.1021/ja306652c | J. Am. Chem. Soc. 2012, 134, 17186−17201

neighbor C7 H-bonds, which make up the remainder of the H-bonded network, point in directions that also largely cancel one another's dipole moment, leading to dipole moments of 2.6 and 2.8 D, for ZG5-OH and ZG5-NHMe, respectively.

In order to better understand this energetic preference for the mixed helix over other prototypical secondary structures for this homoglycine series, we have carried out DFT M05-2X/6-31+G(d) optimizations of these alternative secondary structures for direct comparison with the mixed helix global minima. These results are summarized in Figure 13. In carrying out these calculations, we used Ramachandran angles for the starting structures that are idealized values based on infinite repeating subunits. Included in the comparison are examples of extended $\beta$-strand, $3_1$-helix (PGII), $3_{10}$ helix, and $\beta$-hairpin structures. In many cases, optimization led to a minimum close to this idealized form. However, PGII starting structures underwent significant structural rearrangements, indicating that these structures are not stable minima in the absence of solvent stabilization. The $\beta$-strand is the closest stable analogue to PGI and also serves as a reference for a fully extended structure which possesses no standard H-bonds, but only a sequence of C5 H-bonds that necessarily accompanies the fully extended conformation. Similarly, the $3_1$-helix that is prototypical of PGII optimized to a partially unfolded structure with energy shown in green, with the first two residues in extended form. The two ZG5 $\beta$-strand conformations (in red) are structures that did not converge to a true minimum, but are instead transition state structures along the coordinate of the lowest-frequency vibration (5 $cm^{-1}$ phenyl torsion for ZG5 and 2 $cm^{-1}$ chain flapping for ZG5-NHMe). Given the small magnitude of these imaginary frequencies, it is assumed that the true minimum is not far below that tabulated in Figure 13, considering the scale of the diagram.

One notable aspect of the comparison of these prototypical structures is the magnitudes of the dipole moments, which are included as labels on the plot. As already mentioned, the mixed helices have dipole moments near 2 D, while the periodic structures have dipole moments several times this, due to the fact that the local dipole moments in these repeating structures point in the same direction and thus increase linearly with increasing size. Only in the $\beta$-hairpins, with its antiparallel $\beta$-strand sections, are the dipole moments near the same size as the mixed helices.

Second, the computed results in Figure 13 provide a quantitative estimate of the overall stability of each prototypical structure, and how they develop with increasing size, with the $\beta$-strand serving as a useful reference. In ZG1, this "extended" form is the only option, since intramolecular H-bonds cannot be formed without significant strain. In ZG3, the global minimum is ~25 kJ/mol more stable than the extended $\beta$-strand, due to the C11/C7/C7/$\pi$ H-bonded network. This energy difference increases to 75−80 kJ/mol in ZG5-OH and ZG5-NHMe with the growing size of the H-bonded network, which now consists of 5−6 H-bonds. It would be interesting to submit these structures to fragment molecular orbital pair interaction energy decomposition analysis (FMO/PIEDA), as was done recently for $\gamma$-peptide triamides,[41] in order to better understand the contributions from noncovalent interactions to the stabilization.

By virtue of its network of C10 H-bonds, the $3_{10}$-helix is more stable than the $3_1$-helix; nevertheless, it still is less stable than the mixed helix structures by 35 and 55 kJ/mol in ZG5-NHMe and ZG5-OH, respectively. The greater stability of $3_{10}$ in ZG5-NHMe than in ZG5-OH is due to the presence of one more C10 H-bond in ZG5-NHMe. The $3_1$ helix associated with PGII contains no strong intramolecular H-bonds, receiving much of its stabilization in solution from H-bonds with $H_2O$ that point successive amide groups at angles near 120° relative to one another. Because this orientation is less stable than the all-anti $\beta$-strand, it is calculated to be higher in energy even than the $\beta$-strands, with the minima reached by optimization 96 and 99 kJ/mol higher in energy than the mixed helices for ZG5-OH, and ZG5-NHMe, respectively.

Finally, among the model secondary structures tested, $\beta$-hairpins were closest in energy, with optimized energies 32 and 19 kJ/mol above the mixed helices for ZG5-OH and ZG5-NHMe, respectively. The $\beta$-hairpin in ZG5-OH is a prototypical structure, turned 180° by a $\beta$-turn (involving a C10 ring) and formed into an antiparallel $\beta$-sheet, with the C-terminal OH group reaching back to form a H-bond with the Z-cap C═O group. The "distorted" hairpin in ZG5-NHMe is characterized by a C7 $\gamma$-turn and C11 H-bond which provides the 180° turn needed for $\beta$-sheet formation, but keeping the strands slightly out of plane. Interestingly, of the calculated structures for ZG5-NHMe, this was the sixth from the global minimum.

The results in Figure 13 drive home the point that the mixed helices are energetically far more stable than PGI, PGII, $3_{10}$, and $\beta$-hairpin structures for homoglycines in the gas phase, due both to the network of H-bonds and to their alternating directions that minimize the dipole moment. On the basis of the calculations, even when free energy differences are compared, the mixed helices remain the most stable up to 300 K. This raises the prospect that mixed helices might be viable secondary structures in polyglycines in nonpolar environments.

## 5. CONCLUSION

The conformational preferences of homoglycine sequences in the absence of solvent were addressed in this work via conformation-specific UV and IR spectroscopy for the Z-$(Gly)_n$-OH, $n$ = 1, 3, 5 and Z-$(Gly)_5$-NHMe series. By analyzing in detail the infrared spectra of the observed conformers, structural assignments were made that pointed to a developing secondary structure that by $n$ = 5 has the clear markings of a mixed $H_{14/16}$ helix. The ZG5-OH and ZG5-NHMe pentaglycines each fold into a single conformation comprising about 1.5 turns of such a mixed helix, with C14 and C16 H-bonded rings serving as the primary means by which the turns of the helix are locked in place. Nearest-neighbor C7 rings play a supporting role, providing additional H-bonds that turn the peptide backbone and give it added stability.

These results are noteworthy in several respects. First, in all members of this sequence, but most notably in the pentaglycines ZG5-OH and ZG5-NHMe, the conformational population funnels under jet cooling either primarily (in ZG1 and ZG3) or exclusively (ZG5-OH and ZG5-NHMe) into a single conformational minimum. This occurs despite the fact that the individual glycine residues have open to them larger regions of the Ramachandran plot than any other amino acid, and hence might be expected to be able to form many competing structures with similar energies.

Second, this strongly preferred structure is not one of the secondary structures proposed for polyglycines in solution, crystalline, or fibril form (PGI or PGII), nor a $3_{10}$ helix or $\beta$-strand, but rather a mixed helix. Such mixed helices, with


dx.doi.org/10.1021/ja306652c | J. Am. Chem. Soc. 2012, 134, 17186−17201

alternating H-bond types, are a unique type of secondary structure much more common in synthetic foldamers[63−65] than in $\alpha$-peptides. Nevertheless, Baldauf et al. predicted on the basis of calculations of model capped glycine hexamers that the $H_{14/16}$ mixed helix would be preferred over other common secondary structures. We have provided here the first experimental evidence for their status as a preferred conformation of the isolated polyglycines, albeit in abbreviated form in a structure with a single C14/C16 pair that produces about 1.5 turns of the mixed helix.

Third, one of the characteristic features of the mixed helix structure for ZG5-OH and ZG5-NHMe is their small dipole moment, arising from the cancellation of individual amide dipoles due to the alternating directions of the H-bonds, N → C ($i \rightarrow i + 3$) in the C14 ring and C → N ($i + 5 \rightarrow i$) in the C16 ring. As a result, these structures should be favored in nonpolar environments over other secondary structural types that incorporate repeat subunits that point the amide dipoles in the same direction, leading to macroscopic dipoles with magnitudes far greater than those in the mixed helices (Figure 13). Here, the study of the conformers in isolation in the gas phase provides the ultimate nonpolar environment in which conformer stabilization is due entirely to intramolecular interactions within the peptide itself.

Fourth, the predictions of calculations carried out at the DFT M05-2X/6-31+G(d) level of theory is that the mixed helices have free energies lower than other secondary structures even at 300 K. This raises the tantalizing prospect that these mixed helices could still be preferred in nonpolar environments in the condensed phase, especially if this preference continues to grow with the length of the polyglycine chain. Whether this preference also extends to nonpolar regions of membranes is an open question deserving further study.

Having discovered these mixed helices in the isolated molecules, there are several fruitful avenues worth pursuing in future work. It would seem important to gain a more comprehensive understanding of the potential energy and free energy landscapes, and of the folding pathways that occur in moving between model secondary structures. There is a role here for simulations based on disconnectivity diagrams[61,62,66] that map out the conformational minima, transition states, and pathways much more broadly than is typical.

The single-conformation amide I/II spectra obtained in this work provide an important point of contact with modern theories seeking to predict these spectra without resorting to full *ab initio* calculation. We have recently presented[54] amide I/II spectra from a test set of 21 conformations of model $\alpha$-, $\beta$-, $\gamma$-, and $\alpha/\beta$-peptide-capped diamides and triamides, and used Hessian Reconstruction[67] to extract the uncoupled, local mode frequencies and IR intensities, and amide−amide coupling terms (both amide I/I and amide II/II). From this test set, we deduced that the amide I/I and amide II/II couplings are dictated by the hydrogen bonds that join them. This is a qualitatively different picture than the transition dipole coupling (TDC)[63,68] or transition charge coupling (TCC)[69−73] models that have been used to describe such coupling terms in the past. The ZGly series studied here provide a further testing ground for these methods, the results of which will be reported elsewhere.

Finally, it would be valuable to see how these structural preferences develop as the polyglycine chain is extended beyond $n = 5$ and how it might be modified by the presence of one or a few water molecules bound to the polyglycines. Such strongly bound water molecules are likely to form bridges between amide groups,[74] and could either break up the mixed helix or enhance its formation by stabilizing remaining unbound amide polar groups.

## ■ ASSOCIATED CONTENT

### Supporting Information

The laser desorption scheme used in this work, ZG5-NHMe structural comparison, experimental vibrational frequencies, ZG3 free energy corrections, and ZG1/ZG3/ZG5 structural similarities. This material is available free of charge via the Internet at http://pubs.acs.org.

## ■ AUTHOR INFORMATION

### Corresponding Author

zwier@purdue.edu

### Notes

The authors declare no competing financial interest.

## ■ ACKNOWLEDGMENTS

The authors gratefully acknowledge support for this work from the National Science Foundation (NSF CHE 1213289). The authors also thank Dr. Carsten Baldauf for first pointing out the connection with his work on mixed helices.

## ■ REFERENCES

(1) Lovell, S. C.; Davis, I. W.; Adrendall, W. B.; de Bakker, P. I. W.; Word, J. M.; Prisant, M. G.; Richardson, J. S.; Richardson, D. C. *Proteins* **2003**, *50*, 437−450.
(2) Ho, B. K.; Brasseur, R. *BMC Struct. Biol.* **2005**, 5.
(3) Read, R. J.; Adams, P. D.; Arendall, W. B.; Brunger, A. T.; Emsley, P.; Joosten, R. P.; Kleywegt, G. J.; Krissinel, E. B.; Lutteke, T.; Otwinowski, Z.; Perrakis, A.; Richardson, J. S.; Sheffler, W. H.; Smith, J. L.; Tickle, I. J.; Vriend, G.; Zwart, P. H. *Structure* **2011**, *19*, 1395−1412.
(4) Bamford, C. H.; Brown, L.; Cant, E. M.; Elliott, A.; Hanby, W. E.; Malcolm, B. R. *Nature* **1955**, *176*, 396−397.
(5) Bykov, S.; Asher, S. *J. Phys. Chem. B* **2010**, *114*, 6636−6641.
(6) Bykov, S. V.; Asher, S. A. *J. Phys. Chem. Lett.* **2010**, *1*, 269−271.
(7) Ohnishi, S.; Kamikubo, H.; Onitsuka, M.; Kataoka, M.; Shortle, D. *J. Am. Chem. Soc.* **2006**, *128*, 16338−16344.
(8) Lorusso, M.; Pepe, A.; Ibris, N.; Bochicchio, B. *Soft Matter* **2011**, *7*, 6327−6336.
(9) Lesarri, A.; Cocinero, E. J.; Lopez, J. C.; Alonso, J. L. *ChemPhysChem* **2005**, *6*, 1559−1566.
(10) Kamrath, M. Z.; Garand, E.; Jordan, P. A.; Leavitt, C. M.; Wolk, A. B.; Van Stipdonk, M. J.; Miller, S. J.; Johnson, M. A. *J. Am. Chem. Soc.* **2011**, *133*, 6440−6448.
(11) Leavitt, C. M.; Wolk, A. B.; Kamrath, M. Z.; Garand, E.; Van Stipdonk, M. J.; Johnson, M. A. *J. Am. Soc. Mass Spectrom.* **2011**, *22*, 1941−1952.
(12) Hudgins, R. R.; Mao, Y.; Ratner, M. A.; Jarrold, M. F. *Biophys. J.* **1999**, *76*, 1591−1597.
(13) Wu, R. H.; McMahon, T. B. *J. Phys. Chem. B* **2009**, *113*, 8767−8775.
(14) Wieczorek, R.; Dannenberg, J. J. *J. Am. Chem. Soc.* **2003**, *125*, 14065−14071.
(15) Baldauf, C.; Gunther, R.; Hofmann, H. J. *Angew. Chem., Int. Ed.* **2004**, *43*, 1594−1597.
(16) Baldauf, C.; Gunther, R.; Hofmann, H. J. *Biopolymers* **2005**, *80*, 675−687.
(17) Chaudhuri, P.; Canuto, S. *J. Mol. Struct. (THEOCHEM)* **2008**, *849*, 25−32.
(18) Ferrari, A. M.; Civalleri, B.; Dovesi, R. *J. Comput. Chem.* **2010**, *31*, 1777−1784.

(19) Atwood, R. E.; Urban, J. J. *J. Phys. Chem. A* **2012**, *116*, 1396−1408.
(20) Baldauf, C.; Gunther, R.; Hofmann, H. J. *Helv. Chim. Acta* **2003**, *86*, 2573−2588.
(21) Baldauf, C.; Gunther, R.; Hofmann, H. J. *Biopolymers* **2006**, *84*, 408−413.
(22) Baldauf, C.; Gunther, R.; Hofmann, H. J. *J. Org. Chem.* **2006**, *71*, 1200−1208.
(23) Kulp, J. L.; Clark, T. D. *Chem.—Eur. J.* **2009**, *15*, 11867−11877.
(24) Itoh, S. G.; Okumura, H. *J. Phys. Soc. Jpn.* **2011**, *80*, 094801.
(25) Chin, W.; Compagnon, I.; Dognon, J. P.; Canuel, C.; Piuzzi, F.; Dimicoli, I.; von Helden, G.; Meijer, G.; Mons, M. *J. Am. Chem. Soc.* **2005**, *127*, 1388−1389.
(26) Chin, W.; Piuzzi, F.; Dimicoli, I.; Mons, M. *Phys. Chem. Chem. Phys.* **2006**, *8*, 1033−1048.
(27) Compagnon, I.; Oomens, J.; Bakker, J.; Meijer, G.; von Helden, G. *Phys. Chem. Chem. Phys.* **2005**, *7*, 13−15.
(28) Compagnon, I.; Oomens, J.; Meijer, G.; von Helden, G. *J. Am. Chem. Soc.* **2006**, *128*, 3592−3597.
(29) Gerhards, M.; Unterberg, C. *Phys. Chem. Chem. Phys.* **2002**, *4*, 1760−1765.
(30) Brenner, V.; Piuzzi, F.; Dimicoli, I.; Tardivel, B.; Mons, M. *J. Phys. Chem. A* **2007**, *111*, 7347−7354.
(31) Chin, W.; Piuzzi, F.; Dognon, J. P.; Dimicoli, L.; Tardivel, B.; Mons, M. *J. Am. Chem. Soc.* **2005**, *127*, 11900−11901.
(32) Fricke, H.; Gerlach, A.; Gerhards, M. *Phys. Chem. Chem. Phys.* **2006**, *8*, 1660−1662.
(33) Gerhards, M.; Unterberg, C.; Gerlach, A. *Phys. Chem. Chem. Phys.* **2002**, *4*, 5563−5565.
(34) Plowright, R. J.; Gloaguen, E.; Mons, M. *ChemPhysChem* **2011**, *12*, 1889−1899.
(35) Baquero, E. E.; James, W. H.; Choi, S. H.; Gellman, S. H.; Zwier, T. S. *J. Am. Chem. Soc.* **2008**, *130*, 4784−4794.
(36) Baquero, E. E.; James, W. H.; Choi, S. H.; Gellman, S. H.; Zwier, T. S. *J. Am. Chem. Soc.* **2008**, *130*, 4795−4807.
(37) James, W. H.; Baquero, E. E.; Choi, S. H.; Gellman, S. H.; Zwier, T. S. *J. Phys. Chem. A* **2010**, *114*, 1581−1591.
(38) James, W. H.; Baquero, E. E.; Shubert, V. A.; Choi, S. H.; Gellman, S. H.; Zwier, T. S. *J. Am. Chem. Soc.* **2009**, *131*, 6574−6590.
(39) Buchanan, E. G.; James, W. H.; Gutberlet, A.; Dean, J. C.; Guo, L.; Gellman, S. H.; Zwier, T. S. *Faraday Discuss.* **2011**, *150*, 209−226.
(40) James, W. H.; Buchanan, E. G.; Guo, L.; Gellman, S. H.; Zwier, T. S. *J. Phys. Chem. A* **2011**, *115*, 11960−11970.
(41) James, W. H.; Buchanan, E. G.; Muller, C. W.; Dean, J. C.; Kosenkov, D.; Slipchenko, L. V.; Guo, L.; Reidenbach, A. G.; Gellman, S. H.; Zwier, T. S. *J. Phys. Chem. A* **2011**, *115*, 13783−13798.
(42) Abo-Riziq, A.; Bushnell, J. E.; Crews, B.; Callahan, M.; Grace, L.; De Vries, M. S. *Chem. Phys. Lett.* **2006**, *431*, 227−230.
(43) de Vries, M. S.; Hobza, P. *Annu. Rev. Phys. Chem.* **2007**, *58*, 585−612.
(44) Lubman, L. L. a. D. M. *Appl. Spectrosc.* **1988**, *42*, 411−417.
(45) Meijer, G.; de Vries, M. S.; Hunziker, H. E.; Wendt, H. R. *Appl. Phys. B* **1990**, *51*, 395−403.
(46) Page, R. H.; Shen, Y. R.; Lee, Y. T. *J. Chem. Phys.* **1988**, *88*, 4621−4636.
(47) Zwier, T. S. *J. Phys. Chem. A* **2001**, *105*, 8827−8839.
(48) Weiner, P. K.; Kollman, P. A. *J. Comput. Chem.* **1981**, *2*, 287−303.
(49) Mohamadi, F.; Richards, N. G. J.; Guida, W. C.; Liskamp, R.; Lipton, M.; Caufield, C.; Chang, G.; Hendrickson, T.; Still, W. C. *J. Comput. Chem.* **1990**, *11*, 440−467.
(50) Frisch, M. J.; et al. *Gaussian 09*, revision B.01; Gaussian, Inc.: Wallingford, CT, 2009.
(51) Zhao, Y.; Truhlar, D. G. *J. Chem. Theory Comput.* **2007**, *3*, 289−300.
(52) Dean, J. C.; Buchanan, E. G.; James, W. H.; Gutberlet, A.; Biswas, B.; Ramachandran, P. V.; Zwier, T. S. *J. Phys. Chem. A* **2011**, *115*, 8464−8478.
(53) Stearns, J. A.; Guidi, M.; Boyarkin, O. V.; Rizzo, T. R. *J. Chem. Phys.* **2007**, *127*, 154322.
(54) Buchanan, E. G.; James, W. H., III; Choi, S. H.; Guo, L.; Gellman, S. H.; Müller, C. W.; Zwier, T. S. *J. Chem. Phys.* **2012**, *137*, 094301.
(55) Torii, H. *J. Phys. Chem. Lett.* **2012**, *3*, 112−116.
(56) Rizzo, T. R.; Stearns, J. A.; Boyarkin, O. V. *Int. Rev. Phys. Chem.* **2009**, *28*, 481−515.
(57) Stearns, J. A.; Seaiby, C.; Boyarkin, O. V.; Rizzo, T. R. *Phys. Chem. Chem. Phys.* **2009**, *11*, 125−132.
(58) Southern, C. A.; Levy, D. H.; Stearns, J. A.; Florio, G. M.; Longarte, A.; Zwier, T. S. *J. Phys. Chem. A* **2004**, *108*, 4599−4609.
(59) Gloaguen, E.; de Courcy, B.; Piquemal, J. P.; Pilme, J.; Parisel, O.; Pollet, R.; Biswal, H. S.; Piuzzi, F.; Tardivel, B.; Broquier, M.; Mons, M. *J. Am. Chem. Soc.* **2010**, *132*, 11860−11863.
(60) Shubert, V. A.; Baquero, E. E.; Clarkson, J. R.; James, W. H.; Turk, J. A.; Hare, A. A.; Worrel, K.; Lipton, M. A.; Schofield, D. P.; Jordan, K. D.; Zwier, T. S. *J. Chem. Phys.* **2007**, *127*, 234315.
(61) Becker, O. M.; Karplus, M. *J. Chem. Phys.* **1997**, *106*, 1495−1517.
(62) Wales, D. J. *Energy Landscapes*; Cambridge University Press: Cambridge, 2003.
(63) Krimm, S.; Bandekar, J. *Adv. Protein Chem.* **1986**, *38*, 181−364.
(64) Sharma, G. V. M; Reddy, K. R.; Krishna, P. R.; Sankar, A. R.; Narsimulu, K.; Kumar, S. K.; Jayaprakash, P.; Jagannadh, B.; Kunwar, A. C. *J. Am. Chem. Soc.* **2003**, *125*, 13670−13671.
(65) Vasudev, P. G.; Chatterjee, S.; Shamala, N.; Balaram, P. *Chem. Rev.* **2011**, *111*, 657−687.
(66) Oakley, M. T.; Wales, D. J.; Johnston, R. L. *J. Phys. Chem. B* **2011**, *115*, 11525−11529.
(67) Ham, S.; Cha, S.; Choi, J. H.; Cho, M. *J. Chem. Phys.* **2003**, *119*, 1451−1461.
(68) Torii, H.; Tasumi, M. *J. Chem. Phys.* **1992**, *96*, 3379−3387.
(69) Falvo, C.; Zhuang, W.; Kim, Y. S.; Axelsen, P. H.; Hochstrasser, R. M.; Mukamel, S. *J. Phys. Chem. B* **2012**, *116*, 3322−3330.
(70) Gorbunov, R. D.; Kosov, D. S.; Stock, G. *J. Chem. Phys.* **2005**, *122*, 224904.
(71) Jansen, T. L.; Dijkstra, A. G.; Watson, T. M.; Hirst, J. D.; Knoester, J. *J. Chem. Phys.* **2006**, *125*, 044312.
(72) Maekawa, H.; Ge, N. H. *J. Phys. Chem. B* **2010**, *114*, 1434−1446.
(73) Watson, T. M.; Hirst, J. D. *Mol. Phys.* **2005**, *103*, 1531−1546.
(74) Nagornova, N. S.; Rizzo, T. R.; Boyarkin, O. V. *Science* **2012**, *336*, 320−323.